Identifying the Most (Cost-)Efficient Regions for CO2 Removal With Iron Fertilization in the Southern Ocean

Lennart Bach, Veronica Tamsitt, Kimberlee Baldry, Jeffrey Mcgee, Emmanuel Laurenceau-Cornec, Robert Strzepek, Yinghuan Xie, Philip Boyd

Global Biogeochemical Cycles

RESEARCH ARTICLE
10.1029/2023GB007754

Special Section:
Southern Ocean and Climate: Biogeochemical and Physical Fluxes and Processes

Identifying the Most (Cost-)Efficient Regions for CO_2 Removal With Iron Fertilization in the Southern Ocean

Lennart T. Bach[1], Veronica Tamsitt[2], Kimberlee Baldry[1], Jeffrey McGee[1,3], Emmanuel C. Laurenceau-Cornec[1,4], Robert F. Strzepek[1,5], Yinghuan Xie[1], and Philip W. Boyd[1,5]

[1]Institute for Marine and Antarctic Studies, University of Tasmania, Hobart, TAS, Australia, [2]College of Marine Science, University of South Florida, St. Petersberg, FL, USA, [3]Faculty of Law, University of Tasmania, Hobart, TAS, Australia, [4]CNRS, IRD, Ifremer, LEMAR, University of Brest, Plouzane, France, [5]Australian Antarctic Program Partnership, Hobart, TAS, Australia

Abstract Ocean iron fertilization (OIF) aims to remove carbon dioxide (CO_2) from the atmosphere by stimulating phytoplankton carbon-fixation and subsequent deep ocean carbon sequestration in iron-limited oceanic regions. Transdisciplinary assessments of OIF have revealed overwhelming challenges around the detection and verification of carbon sequestration and wide-ranging environmental side-effects, thereby dampening enthusiasm for OIF. Here, we utilize five requirements that strongly influence whether OIF can lead to atmospheric CO_2 removal (CDR): The requirement (a) to use preformed nutrients from the lower overturning circulation cell; (b) for prevailing iron-limitation; (c) for sufficient underwater light for photosynthesis; (d) for efficient carbon sequestration; (e) for sufficient air-sea CO_2 transfer. We systematically evaluate these requirements using observational, experimental, and numerical data in an "informed back-of-the-envelope approach" to generate circumpolar maps of OIF (cost-)efficiency south of 60°S. Results suggest that (cost-)efficient CDR is restricted to locations on the Antarctic Shelf. Here, CDR costs can be <100 US$/tonne CO_2 while they are mainly >>1,000 US$/tonne CO_2 in offshore regions of the Southern Ocean, where mesoscale OIF experiments have previously been conducted. However, sensitivity analyses underscore that (cost-)efficiency is in all cases associated with large variability and are thus difficult to predict, which reflects our insufficient understanding of the relevant biogeochemical and physical processes. While OIF implementation on Antarctic shelves appears most (cost-)efficient, it raises legal questions because regions close to Antarctica fall under three overlapping layers of international law. Furthermore, the constraints set by (cost-)efficiency reduce the area suitable for OIF, thereby likely reducing its maximum CDR potential.

Key Points:

- Iron fertilization efficiency is constrained mainly by carbon transfer efficiency into Antarctic Bottom Water and air-sea CO_2 exchange
- Iron fertilization could cost below 100 US-Dollar per tonne CO_2 on Antarctic shelves but may be much more expensive off shelves
- (Cost-)efficient Iron Fertilization is restricted to relatively small parts of the Southern Ocean that are protected by international law

Supporting Information:

Supporting Information may be found in the online version of this article.

Correspondence to:

L. T. Bach,
lennart.bach@utas.edu.au

Citation:

Bach, L. T., Tamsitt, V., Baldry, K., McGee, J., Laurenceau-Cornec, E. C., Strzepek, R. F., et al. (2023). Identifying the most (cost-)efficient regions for CO_2 removal with iron fertilization in the Southern Ocean. *Global Biogeochemical Cycles*, *37*, e2023GB007754. https://doi.org/10.1029/2023GB007754

Received 28 FEB 2023
Accepted 26 OCT 2023

Author Contributions:

Conceptualization: Lennart T. Bach, Philip W. Boyd
Data curation: Lennart T. Bach, Emmanuel C. Laurenceau-Cornec, Robert F. Strzepek

1. Introduction

Restricting global warming to 1.5°C requires atmospheric carbon dioxide (CO_2) removal of 100–1,000 gigatonnes (Gt) until 2,100 as a supplement to the rapid emission reduction (Rogelj et al., 2018). It has been proposed that gigatonne-scale CO_2 removal (CDR) can be realized by using a portfolio of methods, but they generally lack technological readiness (Nemet et al., 2018). Ocean iron fertilization (OIF) is a widely considered method within the marine CDR portfolio. OIF aims to stimulate CO_2 fixation by marine phytoplankton through the addition of dissolved iron (DFe) to nutrient-rich (nitrate, phosphate) but iron-limited surface ocean regions, mainly in the Southern Ocean or in low iron regions of the Pacific Ocean. The rationale for CDR is that a significant proportion of the additional CO_2 fixed in phytoplankton biomass will then sink into the deep ocean, where the carbon (C) could be sequestered for centuries to millennia (Martin, 1990). Indeed, paleo-oceanographic evidence suggests that changes in iron delivery to the surface ocean via dust and the associated enhancement of deep ocean CO_2 sequestration could explain around 25% of the 80 ppmv glacial-interglacial atmospheric CO_2 transitions (Martínez-García et al., 2014).

Research into OIF commenced in the 1980's and was largely informed by 13 mesoscale iron fertilization experiments (Yoon et al., 2018), which aimed to answer fundamental questions in climate science (Martin, 1990). Today, OIF is arguably the most thoroughly assessed open ocean CDR method, having undergone scrutiny by transdisciplinary international research efforts. The early enthusiasm for OIF faded with increasing understanding of the complexity of the method and growing concerns around environmental side-effects (Buesseler, 2012; de Baar et al., 2005; Gattuso et al., 2018; Rohr, 2019; Strong et al., 2009). However, despite justified skepticism, OIF is still considered as a potential addition to the CDR portfolio needed to achieve net zero goals (Fuss

Formal analysis: Lennart T. Bach, Veronica Tamsitt, Kimberlee Baldry, Jeffrey McGee, Emmanuel C. Laurenceau-Cornec, Robert F. Strzepek, Yinghuan Xie, Philip W. Boyd
Funding acquisition: Philip W. Boyd
Investigation: Lennart T. Bach, Veronica Tamsitt, Kimberlee Baldry, Philip W. Boyd
Methodology: Lennart T. Bach, Kimberlee Baldry, Emmanuel C. Laurenceau-Cornec
Project Administration: Philip W. Boyd
Resources: Emmanuel C. Laurenceau-Cornec
Software: Veronica Tamsitt, Kimberlee Baldry
Supervision: Veronica Tamsitt
Validation: Lennart T. Bach, Veronica Tamsitt, Emmanuel C. Laurenceau-Cornec, Yinghuan Xie, Philip W. Boyd
Visualization: Lennart T. Bach, Veronica Tamsitt, Kimberlee Baldry, Yinghuan Xie
Writing – original draft: Lennart T. Bach
Writing – review & editing: Lennart T. Bach, Veronica Tamsitt, Kimberlee Baldry, Jeffrey McGee, Emmanuel C. Laurenceau-Cornec, Robert F. Strzepek, Yinghuan Xie, Philip W. Boyd

et al., 2018) and there is renewed interest in large-scale scientific assessment of this CDR method (Buesseler et al., 2023; Emerson, 2019; NASEM, 2021; Oeste et al., 2017; Yoon et al., 2018).

Simulations with biogeochemical model project that continuous basin-scale or globally-applied OIF could sequester around 2–4 Gt CO_2 $year^{-1}$ (Aumont & Bopp, 2006; Fu & Wang, 2022; Oschlies et al., 2010; Tagliabue et al., 2023; Zahariev et al., 2008). However, OIF would likely not be achievable at such a large scale due to environmental concerns, associated legal constraints and hence difficulties in obtaining social license (Cox et al., 2021; Strong et al., 2009). Indeed, the same modeling studies have highlighted negative side-effects of large scale and continuous Southern Ocean OIF deployments, such as so-called "nutrient robbing" by OIF upstream (i.e., poleward in the Southern Ocean) from low-latitude regions, water column deoxygenation, and the formation of more potent greenhouse gasses in oxygen-depleted waters (Aumont & Bopp, 2006; Fu & Wang, 2022; Oschlies et al., 2010; Tagliabue et al., 2023; Zahariev et al., 2008). Furthermore, the outcomes of some model simulations have suggested that targeting particular regions or seasons could optimize the CDR efficiency of OIF (Arrigo & Tagliabue, 2005; Fu & Wang, 2022; Gnanadesikan & Marinov, 2008; Gnanadesikan et al., 2003; Sarmiento et al., 2010). For example, Sarmiento et al. (2010) simulated OIF at two sites in the Pacific and two sites in the Southern Ocean. They found substantially higher CDR efficiencies in the Southern Ocean, in particular in the Ross Sea (Sarmiento et al., 2010). Their findings suggest that OIF would more likely become a meaningful addition to the global CDR portfolio when deployed in locations of the Southern Ocean where its CDR efficiency (i.e., CDR per added iron) is highest and costs (i.e., costs per tonne (t) CO_2 removed) are lowest. (Cost-)efficiency is among the most decisive factors influencing whether stakeholders (which may be countries or private enterprises) pursue real-world implementation of OIF (Bellamy & Geden, 2019; Rickels et al., 2012).

Our study builds on previous modeling research and aims to refine our understanding of Southern OIF by providing a spatially resolved (~1° grid resolution) circumpolar analysis of CDR- and cost-efficiency south of 60°S. As such, we aim to further the debate on OIF by narrowing down where OIF is biogeochemically and economically feasible. The structure and goals of the study are illustrated and described in Figure 1. After the methods section, we begin by evaluating five requirements that largely determine whether OIF may be feasible in certain areas and how this requirement affects the efficiency of OIF (Section 3.1). Next, we present maps of CDR efficiency and OIF costs in the Southern Ocean south of 60°S (Section 3.2.) and discuss the variability of OIF (cost-)efficiency (Section 3.3.). Finally, we discuss the legal ramifications (Section 3.4.) and synthesize the key findings of this study (Section 4).

2. Methods

2.1. Justification for the Applied Methodology

Our approach differs from previous numerical assessments of OIF in that we do not employ a biogeochemical model for our research. Instead, we employ a range of observational, experimental, and computational data sources to assemble the necessary information and compile it in equations to derive estimates of OIF cost-efficiency. Our approach is therefore less comprehensive and internally consistent than a biogeochemical model as it omits a variety of processes and draws information from different sources. This "informed back-of-the-envelope approach" was chosen to achieve the goals of the study (Figure 1) mainly for two reasons. First, due to findings by Sarmiento et al. (2010) we focused our analysis on south of 60°S where Antarctic Bottom Water (AABW) formation is a predominant driver of OIF efficiency. Biogeochemical models have limited skill to reproduce AABW formation pathways (Heuzé, 2021), so that using them for a circumpolar localization of cost-efficient OIF regions would not have been robust. Second, we considered air-sea CO_2 flux as a potential limitation of OIF efficiency due to the reasons described in Gnanadesikan and Marinov (2008). Models can be used to provide the necessary insights through forward tracking of CO_2 deficient seawater (Bach et al., 2023), but the spatial resolution attempted here would have made this prohibitively expensive. We acknowledge the limitations of our approach as mentioned in the individual method descriptions below.

2.2. Iron Limitation and Light Limitation South of 60°S

To determine the onset of iron-limitation for phytoplankton communities south of 60°S, we synthesized published shipboard iron-amendment experiments via literature analysis (Text S1 in Supporting Information S1). Growth rates (μ) of natural communities of iron-replete (+Fe) conditions were compared with μ in iron-deplete (−Fe)

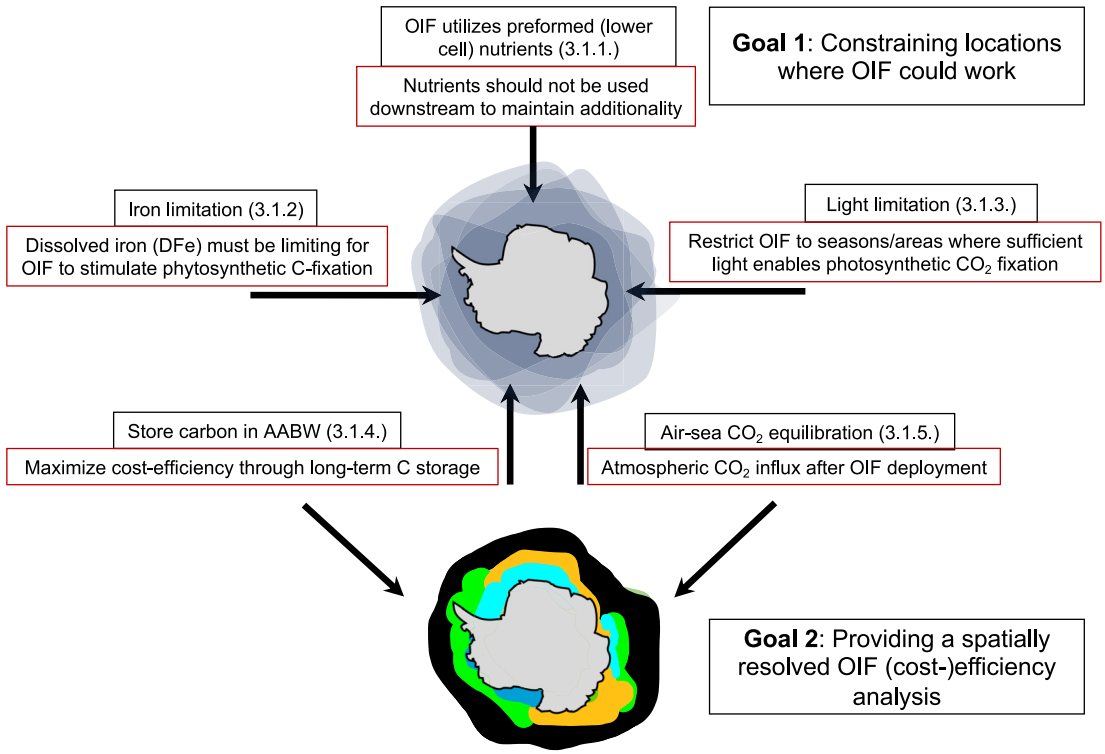

Figure 1. Outline and the two major goals of the ocean iron fertilization (OIF) analysis. Goal 1 is to assess the five requirements that should be met (or maximized) for OIF to be meaningful and/or (cost-)efficient. The value of this exercise is to localize areas in the Southern Ocean where OIF could be more or less effective. Goal 2 is to provide circumpolar maps of OIF (cost-)efficiency. Three of the five requirements in the focus here (pre-formed nutrients, iron limitation, light limitation) are used only to help constrain suitable OIF areas but these are not further considered for the analysis of OIF (cost-)efficiency, due to the reasons described in Sections 3.1.1–3.1.3. The other two of the five requirements (carbon storage in AABW, air-sea CO_2 equilibration), are utilized also for estimating OIF (cost-)efficiency.

communities. We calculated the fold change of growth rate and plotted μ_{+Fe}/μ_{-Fe} as a function of the in situ background (i.e., pre-treatment) DFe concentration from the batch of seawater which was incubated (Table S1 in Supporting Information S1). The bioavailability of DFe was not considered as this was seldom reported in the literature.

Potential light limitation of phytoplankton growth south of 60°S during summer (December-February) was calculated using the observation-based approach developed by Venables and Moore (2010). Satellite and Argo float data were used to calculate the mean irradiance in the surface mixed layer (I_{MLD}) and compare this to the threshold irradiance above which phytoplankton communities can grow (I_{MLD_min}). Venables and Moore (2010) determined an I_{MLD_min} of 3 mol photons m^{-2} d^{-1} for phytoplankton downstream of the Kerguelen Islands. To further constrain I_{MLD_min}, we explored the literature (Text S2 in Supporting Information S1) for growth versus irradiance curves with Southern Ocean phytoplankton species (Table S2 in Supporting Information S1) and fitted a growth versus irradiance model (Eilers & Peeters, 1988) to the binned data to determine the irradiance that corresponds to the onset of irradiance saturation.

2.3. Virtual Particle Tracking in a High-Resolution Physical Ocean Model

We used the output from MOM01 (Morrison et al., 2020), an ocean sea-ice model based on version 5 of the Modular Ocean Model code (Griffies, 2012) for several specific aspects addressed in this study. The model has 1/10° horizontal resolution and 75 vertical levels extending over the full ocean depth, with a vertical resolution in the top 1,000 m ranging from 1.1 m at the surface to 94 m at 1,000 m depth. The atmospheric forcing is derived from version 2 of the Coordinated Ocean-ice Reference Experiments-Normal Year Forcing (CORE-NYF) reanalysis (Large & Yeager, 2009). Sea surface salinity is restored to seasonally varying climatology on 60 day timescale with a piston velocity of 0.16 m day^{-1}. The model does not include ice shelf cavities or tides, and glacial meltwater is input at the sea surface. The model was spun up for 80 years with repeated annual forcing, and then 10 years of daily averaged output was saved for analysis.

We conducted a virtual particle tracking experiment using the Connectivity Modeling System Lagrangian code (CMS, Paris et al., 2013) with daily averaged three-dimensional velocity fields from the first year of MOM01 output. In our simulation, 238,221 neutrally-buoyant virtual particles were seeded on 3 January at 0.5 m depth in each model horizontal grid box south of 60°S and advected forward in time for 1 year with the MOM01 velocity fields. Particles were advected with a timestep of 90 min using a fourth order Runge-Kutta scheme to calculate particle advection, applied in both space and time and particles were reflected at topography or the sea surface. Particle trajectory positions were saved every 5 days and MOM01 temperature and salinity fields were saved along each particle trajectory. We note that the velocity fields used for advecting the particles do not explicitly include mixed layer convection or interior diffusive mixing processes, which affect the movement of tracers. This is a limitation of the chosen method; however, running online Eulerian tracer releases in the model is prohibitively expensive. We further discuss the potential implications of this limitation on the results of the particle tracking experiment in Section 3.1.4.

We utilized particle trajectories to estimate how far particles drift horizontally from the release location within 1 month of simulation and for the calculations of air-sea CO_2 exchange.

2.4. Equilibration of OIF-Derived Seawater CO_2 Deficit With Atmospheric CO_2

There is a risk that OIF reduces CO_2 concentrations in seawater, but the water parcel carrying this CO_2 deficit subducts below the sea surface before CO_2 equilibration with the atmosphere has been completed. In such a case, atmospheric CO_2 removal is delayed potentially far into the future when the CO_2-deficient water is re-exposed to the atmosphere (Bach et al., 2023; He & Tyka, 2023). To investigate this risk, we simulated a Lagrangian experiment for the temporal evolution of a 35 μmol kg^{-1} deficit in dissolved inorganic carbon (DIC), which is typical of OIF experiments with shallow mixed layers of ∼40 m during summer (de Baar et al., 2005; Krishnamurthy et al., 2008). A detailed description of calculations for this bucket approach is provided in Text S3 and Figure S1 in Supporting Information S1. Briefly, a water parcel carrying the CO_2 deficit is represented by the trajectories of neutrally-buoyant virtual particles released in January from MOM01 (Section 2.3). The CO_2-deficient water parcels spread horizontally (following the virtual particle trajectories) and can exchange CO_2 with the atmosphere for as long as the particles are in the mixed layer. Hence, these CO_2-deficient water parcels can be thought of as "buckets," which are initially empty and can fill up with maximally 35 μmol/kg atmospheric CO_2 until the bucket subducts below the mixed layer. The extent to which the bucket is full at the time of exiting the mixed layer (f_{Eq}) is the target variable of this calculation. Air-sea CO_2 influx into the "buckets" is calculated along their trajectories using climatological data (Table S3 in Supporting Information S1). We compare the air-sea CO_2 exchange in an unperturbed "no-OIF scenario" with the exchange in an "OIF scenario." In the calculation, the no-OIF scenario is the expected biogeochemical state along the particle trajectory. The no-OIF scenario allows us to account for changes in air-sea gas exchange due to expected background changes in the carbonate system (i.e., variability in water mass mixing, sea-ice changes and biology). The OIF scenario is the alternate state along a particle trajectory representing an initial DIC deficit of 35 μmol kg^{-1} following OIF and the subsequent change caused by CO_2 exchange with the atmosphere.

2.5. Estimates of CDR Efficiency Using OIF

We refined an equation originally derived by Harrison (2013) to estimate how much of the CO_2 fixed by phytoplankton is transferred into AABW and can be considered as CDR in t C km^{-2} for time-scales of AABW re-ventilation to the atmosphere (i.e., likely >>100 years; England, 1995; Siegel et al., 2021). This equation is composed of five parts (I–V), introduced in the five following paragraphs and combined into one equation thereafter.

Part I estimates the particulate organic carbon (POC) build-up (t C km^{-2}) within a patch of water after iron fertilization:

$$\mathrm{POC} = 1.5 \times \mathrm{MLD} \times \mathrm{C/Fe} \times \frac{12}{1,000,000} \quad (1)$$

Based on previous in situ experiments we assume that OIF increases DFe by 1.5 nM above background concentrations (de Baar et al., 2005) in a patch of 1 km^2 and a given mixed layer depth (MLD) in meters. POC in this

patch then depends on the carbon-to-iron molar elemental ratio (C/Fe) of phytoplankton organic matter, which we assumed to be 25,000 (de Baar et al., 2005; Twining et al., 2004) to reduce the risk of overestimating the CDR potential of OIF. Please note that we neglect the formation of dissolved organic carbon (DOC) here, but note that entrainment of DOC into AABW would make OIF more efficient and reduces costs.

Part II estimates the fraction of the POC produced in the surface (Equation 1) reaching a depth ($z \geq 100$ m (POC_z) as

$$POC_z = POC * e - ratio * \left(\frac{z}{100}\right)^{-b} \quad (2)$$

where the export-ratio (e-ratio) is the fraction of primary production sinking below 100 m (between 0 and 1), and b is the flux attenuation (Martin et al., 1987). The e-ratio and b-values were empirically determined and were compiled from the literature and by using satellite primary production products for the Southern Ocean south of 60°S (see Tables S4 and S5 for further details in Supporting Information S1 and Laurenceau-Cornec et al., 2023). The 122 e-ratios ranged from 0.005 to 0.96 with a median of 0.28 (Table S4 in Supporting Information S1). The 31 b-values ranged from 0.25 to 1.97 with a median of 0.96 (Table S5 in Supporting Information S1). POC_{AABW} is the specific case where POC_z is calculated for the surface depth of AABW. This spatially variable depth horizon (Figure 4f) was chosen as the target depth because we consider POC sinking into AABW to be sequestered for relatively long timescales (discussed in Section 3.1.4). The depth of the upper interface of the AABW layer was defined here as the time-mean depth of the $\sigma_1 = 32.56$ isopycnal surface in the MOM01 model.

Part III (f_{Seq}) assesses how much of the OIF-derived POC that reaches the AABW surface layer (POC_{AABW}) is matched with the influx of atmospheric CO_2. The rationale for this metric is that not all CO_2 consumed by phytoplankton during the OIF-induced bloom must be matched with atmospheric CO_2 because much of it will be respired in and near the surface within weeks (Boyd et al., 2004). Thus, only the "sequestered" POC fraction (i.e., POC_{AABW}) must be matched as this is the amount of POC accounted for as CDR (see below). f_{Seq} was calculated as

$$f_{Seq} = f_{Eq} \div \left(\frac{POC_{AABW}}{POC}\right) \quad (3)$$

Here, $f_{Seq} \geq 1$ means that POC_{AABW} is fully matched with atmospheric CO_2 influx, while any value <1 suggests that air-sea CO_2 has only been partially sequestered (by the fraction between 0 and 1).

Part IV describes how much of the reduction of radiative forcing through CDR is offset through the production of nitrous oxide (N_2O), a greenhouse gas that can be produced following OIF, for example, via nitrification (Law & Ling, 2001):

$$N_2O_{offset} = f_{N_2O} \times POC \times e \times \left(1 - \left(\frac{z_{AABW}}{100}\right)^{-b}\right) \quad (4)$$

Here, f_{N_2O} is the N_2O offset factor, which was determined to be 0.13 ± 0.06 (i.e., $13 \pm 6\%$ of the CDR generated by OIF needs to be discounted by the N_2O feedback (Jin & Gruber, 2003)). The offset was chosen as it was specifically estimated for a Southern OIF (Jin & Gruber, 2003). The dependency on POC sequestration assumes that this discount only needs to be subtracted if the POC is remineralized in a water mass that quickly re-exposes the N_2O to the atmosphere. Thus, no discount occurs when POC reaches AABW where the forming N_2O gas would be sequestered for longer timescales.

Part V ($O_{transport}$) is the CDR offset related to the combustion of fuels for transporting and distributing the iron to the Southern Ocean. It is based on the assumption that a suitable ship for OIF emits ~1.7 t C d^{-1} (Harrison, 2013). Accounting for iron transport and distribution (see following section) yields a value of 0.01 t C km^{-2} of fertilized area (Harrison, 2013).

By combining parts I–V we yield the following equation to calculate CDR:

$$CDR = POC_{AABW} \times f_{Seq} - N_2O_{offset} - O_{transport} \quad (5)$$

The equation was applied to determine spatially resolved CDR, as shown in Figure 5a. Please note that we converted CDR from t C km^{-2} to t CO_2 km^{-2} by multiplication with 3.67.

2.6. Costs of OIF

To estimate OIF costs in \$US t^{-1} CO_2 sequestered in AABW, we first needed to determine operational costs. These were defined as the sum of costs for Fe fertilizers, transport, and distribution in the Southern Ocean.

One operational challenge for OIF is that relatively small amounts of Fe have to be distributed over large areas. Therefore, small vessels are more economical to distribute the Fe within the summer season as larger ships are not fast enough to distribute their load in summer. Following Harrison (2013), we consider a vessel with a payload of 100 t and an optimal speed of 16.7 km hr^{-1}. Such a vessel can fertilize 272 km^2 d^{-1} ($fert_{area}$) at operational costs ($costs_{op}$) of 5,000 \$US d^{-1} (Harrison, 2013). The vessel would need to sail to the fertilization location before and after the OIF operation and need to be restocked for 3 days ($harbor_{time}$). The Fe fertilizer is iron (II) sulfate heptahydrate which costs 600 \$US t^{-1} ($costs_{Fe}$) (Harrison, 2013). The fraction of iron by weight is 0.2 in iron (II) sulfate heptahydrate (Boyd et al., 2000) and the molecular weight (mol_{weight}) of iron is 55.845 g mol^{-1}. Only 50% (i.e., a fraction of 0.5) of iron becomes bioavailable while the remaining 50% is scavenged and sinks out (Bowie et al., 2001). The vessel requires time ($fert_{time}$) to enrich the surface mixed layer by 1.5 nM ($fert_{conc}$) depending on the vessel speed. For our calculation, we used a MLD of 32.8 m, which is the summer (December-February) average south of 60°S computed from Argo float climatology (Holte et al., 2017). Under the above circumstances, the fertilized volume ($fert_{volume}$) can be calculated as

$$\mathrm{fert}_{\mathrm{volume}} = \mathrm{fert}_{\mathrm{area}} \times \mathrm{MLD} \tag{6}$$

Which is 8.92 km^3 d^{-1} in our scenario. This would require a daily amount of iron fertilizer (Fe_{fert}) 7.48 t d^{-1} calculated as

$$\mathrm{Fe}_{\mathrm{fert}} = \mathrm{fert}_{\mathrm{volume}} \times \mathrm{fert}_{\mathrm{conc}} \times \frac{0.5 \times \mathrm{mol}_{\mathrm{weight}}}{0.2} / 1,000 \tag{7}$$

where 1,000 is to convert this to t d^{-1}. Thus, the payload of the ship would be distributed in 27 days ($fert_{time}$) calculated as

$$\mathrm{fert}_{\mathrm{time}} = \frac{\mathrm{payload}}{\mathrm{Fe}_{\mathrm{fert}}} \tag{8}$$

With harbor time (3 days) and sailing back and forth 1,800 km (distance from Tasmania to 60°S) to the OIF site (~16 days), the entire cycle ($cycle_{time}$) takes 46 days calculated as

$$\mathrm{cycle}_{\mathrm{time}} = \mathrm{fert}_{\mathrm{time}} + \mathrm{habor}_{\mathrm{time}} + \mathrm{sailing}_{\mathrm{time}} \tag{9}$$

The costs per fertilized km^2 ($costs_{area}$) are 51 \$US km^{-2} calculated as

$$\mathrm{costs}_{\mathrm{area}} = \frac{\mathrm{cycle}_{\mathrm{time}} \times \mathrm{costs}_{\mathrm{op}} + (\mathrm{payload} \times \mathrm{costs}_{\mathrm{Fe}})}{\mathrm{fert}_{\mathrm{time}} \times \mathrm{fert}_{\mathrm{area}}} \tag{10}$$

We further explored the range of operational $costs_{area}$ within the framework of the above calculation by varying some crucial input assumptions ($costs_{op}$, $costs_{Fe}$, fraction of inorganic particle sinking, Table S6 in Supporting Information S1). This sensitivity test revealed that $costs_{area}$ ranged between 39 and 145 \$US km^{-2} for optimistic to more pessimistic assumptions (Table S6 in Supporting Information S1). Finally, the costs of CDR per t of CO_2 sequestered in AABW (US t^{-1} CO_2) were calculated as

$$\mathrm{Costs}_{\mathrm{tonne}} = \frac{\mathrm{costs}_{\mathrm{area}}}{\mathrm{CDR}}. \tag{11}$$

For the spatial analysis of $Costs_{tonne}$, we use intermediate $costs_{area}$ from Table S6 in Supporting Information S1 (74 \$US km^{-2}).

2.7. Variability of Carbon Export, CDR, and OIF Costs

We conducted Monte Carlo simulations to assess the variability in carbon export, CDR, and OIF costs. These simulations are constrained by the available data.

The amount of POC reaching any given depth (POC_z) can be calculated using Equation 2. Here, e-ratios and b are the sources of variability. To assess the variability of POC_z, we first generated 1,000 e-ratios mimicking their

positively skewed distribution that was found when plotting the 122 compiled values (Table S4 in Supporting Information S1) in a histogram. For this positively skewed distribution, we used a Q-Weibull code in R: q-Weibull (runif(1,000), shape = 1.7, scale = 0.4). Next, we generated 1,000 normally distributed *b*-values mimicking the distribution of the 31 empirically determined *b*-values (Table S5 in Supporting Information S1) as rnorm(1,000, mean = 1.006, sd = 0.385). The 1,000 e-ratios and *b*-values were randomly combined in Equation 2 to yield the distribution of carbon flux attenuation curves and the distribution of POC_z at four different depth horizons.

A systematic assessment for the predominant drivers of variability in CDR was achieved using Equation 5. We first tested which of the components in Equation 5 has the highest capacity to induce variability in CDR. Therefore, we varied each component individually for 1,000 hypothetical cases within their data constraint ranges while keeping the other components constant at their mean values. The parameters individually varied were (a) The C/Fe ratio in phytoplankton with a mean of 25,000 (mol:mol) and a range from 15,000 to 50,000 based on measurements by Twining et al. (2004); (b) POC_{AABW} based on variability in e-ratio and *b* as explained in the previous paragraph; (c) f_{N_2O} with a mean of 0.13 (factorial offset) and a range from 0.07 to 0.21, based on estimates by Jin and Gruber (2003); $O_{transport}$ with a mean offset of 0.044 tonne CO_2 km^{-2} and a range from 0.022 to 0.066, assuming 0.5–1.5 times more or less fuel-efficient transport, for example, via technological improvements or the use of less efficient fuels. For C/Fe, f_{N_2O} and $O_{transport}$, values varied randomly (1,000 cases) within the entire ranges introduced above using a "runif" function in *R* (e.g., C/Fe = runif(1,000, 15,000, 50,000)). Last, all ranges were combined in one calculation to estimate the variability in CDR when all data-constraint ranges in C/Fe, POC_{AABW}, f_{N_2O} and $O_{transport}$ are considered at the same time. Please note that each Monte Carlo simulation was performed for four scenarios: with high (a) and low (0.5) f_{Seq} and for shallow (200 m) and deep (1,000 m) surface depth of AABW. These four scenarios shall be illustrative of the different (and non-random) boundary conditions for air-sea CO_2 influx (Section 3.4) and AABW surface layer depth on the Antarctic shelves and off the shelves in the open Southern Ocean.

Finally, we estimated variability in CDR costs with Equation 11. Therefore, operational costs (Section 2.6) were varied across the range determined in the sensitivity analysis, that is, randomly with 1,000 cases between 39 and 145 $US km^{-2} (Table S6 in Supporting Information S1). This variability in operational cost was then combined in Equation 11 with the variability in CDR costs from the scenario where variability in C/Fe, POC_{AABW}, f_{N_2O} and $O_{transport}$ is considered at the same time.

2.8. Assessment of Legal Constraints

Different international treaties, including those of the Antarctic Treaty System, could affect the implementation of OIF in the Southern Ocean south of 60°S. We reviewed these treaties using international legal analysis to reveal those that explicitly or implicitly consider OIF. The regions for which these treaties apply were subsequently mapped to illustrate where in the Southern Ocean legal challenges can be expected.

3. Results and Discussion

3.1. Five Requirements for the (Cost-)Efficiency of OIF in the Southern Ocean

In the following five Sections 3.1.1–3.1.5, we discuss five requirements that should be met to make OIF feasible and/or more (cost-)efficient. We outline why these requirements are important and assess where in the Southern Ocean they are likely to be met. Each section concludes with whether each requirement is considered for the (cost-)efficiency analysis. Please note that the selection of requirements is meant to cover predominant factors influencing OIF feasibility and (cost-)efficiency, based on our presently available knowledge. However, there may be other factors which are currently unknown or not specifically considered here.

3.1.1. Requirement 1: Nutrient Supply From the Lower Overturning Circulation Cell

So-called "nutrient robbing" has been discussed as a biogeochemical side-effect reducing the efficiency of OIF (The Royal Society, 2009). Nutrient robbing means that CO_2 sequestration stimulated by OIF enables biological drawdown of nutrients such as nitrate (N) and phosphate (P), which are no longer available to fuel CO_2 sequestration downstream of the OIF site (Aumont & Bopp, 2006; Gnanadesikan et al., 2003; Hauck et al., 2018; Oschlies et al., 2010; Sarmiento & Orr, 1991; Tagliabue et al., 2023).

In the Southern Ocean, the reduction of OIF-efficiency due to nutrient robbing can be minimized by restricting the application of OIF to locations south of the Southern Ocean Biogeochemical Divide (SOBD), which is the boundary between the upper and the lower overturning circulation cells in the surface ocean (Marinov et al., 2006;

Sarmiento et al., 2010; Figure 2a). Upwelled nutrients north of the SOBD support downstream primary production north of 30°S (Hauck et al., 2018; Marinov et al., 2006; Palter et al., 2010; Primeau et al., 2013). Thus, CO_2 sequestration through the OIF north of the SOBD in the Southern Ocean would be reduced due to reductions in CO_2 sequestration outside the Southern Ocean at a later point in time (Gnanadesikan & Marinov, 2008; Oschlies et al., 2010; Primeau et al., 2013; Sarmiento et al., 2010). In contrast, nutrient robbing is reduced when OIF is operated south of the SOBD (Sarmiento et al., 2010). Here, upwelled nutrients move (net)southward so that the fraction of nutrients that remains unutilized by phytoplankton becomes entrained in Dense Shelf Water (DSW), the precursor of AABW (Figure 2a). These unutilized nutrients, also known as preformed nutrients (Ito & Follows, 2005), are trapped in the deep ocean circulation cell and therefore not available to fuel downstream primary production, simply because they are not exposed to sunlight outside the Southern Ocean. (Please note that this simplified scheme of an isolated lower overturning circulation cell neglects exchange of water and nutrients with the upper overturning cells, which has to the best of our knowledge not been quantified so far.)

The location of the SOBD has not been well constrained, possibly because the lower-resolution biogeochemical models used to derive and validate the conceptual framework of the SOBD (Marinov et al., 2006; Primeau et al., 2013) often have limited skill to correctly reproduce AABW formation pathways (Heuzé, 2021). To narrow this knowledge gap, Xie et al. (2022) utilized a 1/10° physical model (ACCESS-OM2-01) with good skill at reproducing AABW formation via DSW pathways (Moorman et al., 2020; Morrison et al., 2020) to constrain the geographical location of the SOBD. In this accompanying study, we found that the SOBD constitutes a circumpolar ring relatively close to Antarctica (Figure 2b), shaped by several oceanographic features. Regions south of the SOBD consist mostly of the continental shelves and extend slightly off the shelves in Eastern Antarctica where no in situ OIF experiment has been conducted so far (Figure 2b). The results by Xie et al. (2022) suggest that OIF should be conducted in the blue areas mapped in Figure 2b. Here, nutrient robbing and the associated reduction of (cost-)efficiency would be minimized. Thus, we assume no reduction of OIF (cost-)efficiency in our analysis (Section 3.2.) because OIF would be conducted south of the SOBD.

3.1.2. Requirement 2: Prevailing Iron Limitation

The first step in OIF is the stimulation of phytoplankton C-fixation by the fertilization of the surface ocean with iron. The fertilization can only have a stimulatory effect when iron is limiting C-fixation. Results synthesized here show that phytoplankton are not limited by DFe when concentrations are >0.5 nM. Signs of iron-limitation (i.e., reduced growth) start to become apparent between >0.25 and 0.5 nM, while pronounced reduction of growth is widespread between 0 and 0.25 nM (Figure 3a), highly consistent with DFe thresholds calculated during a mesoscale OIF study using fluorometry (Boyd & Abraham, 2001). Comparing these thresholds to in situ DFe concentrations suggests generally limiting DFe concentrations in Western Antarctica (Figure 3b), consistent with recent findings (Huang et al., 2022). Data coverage in Eastern Antarctica is sparse, although the few observations in the Davis Sea imply less limiting DFe conditions (Figure 3b). Regions with sufficient temporal coverage such as the Ross Sea indicate iron-limited conditions from December to February (Figure S4 in Supporting Information S1). The results of the analysis suggest that OIF would generally stimulate primary production in summer, although natural DFe available early in the growth season may require the postponement of purposeful iron additions until the natural pool has been used up (Arrigo & Tagliabue, 2005). We conclude that iron limitation generally prevails south of 60°S during summer (and is currently increasing; Ryan-Keogh et al., 2023) and therefore not further consider this aspect in the analysis of (cost-)efficiency.

3.1.3. Requirement 3: Absence of Phytoplankton Light Limitation

Low light availability is often considered another potential factor limiting or co-limiting phytoplankton growth in the Southern Ocean even during summer (Venables & Moore, 2010). In cell cultures, light becomes limited for several Southern Ocean phytoplankton species (on average) at 1.5 mol photons m^{-2} d^{-1} (Figure 3c). This value is lower than the threshold for phytoplankton growth (3 mol photons m^{-2} d^{-1}) determined by Venables and Moore (2010) further north in the Southern Ocean. The mean mixed layer irradiance (I_{MLD}) during summer (December-February) was generally well above both of these thresholds, although there are noticeable gaps in the I_{MLD} coverage due to limited float observations near the shelves of Antarctica (Figure 3d). Accordingly, light should generally not limit phytoplankton growth during summer south of 60°S (Figure 3d), which is in line with regional case studies including mesoscale experiments (Boyd et al., 2000). This trend suggests that OIF stimulates primary production south of 60°S during summer when iron is (mildly) limiting phytoplankton growth. As such, we do not consider light limitation for the analysis of OIF (cost-)efficiency.

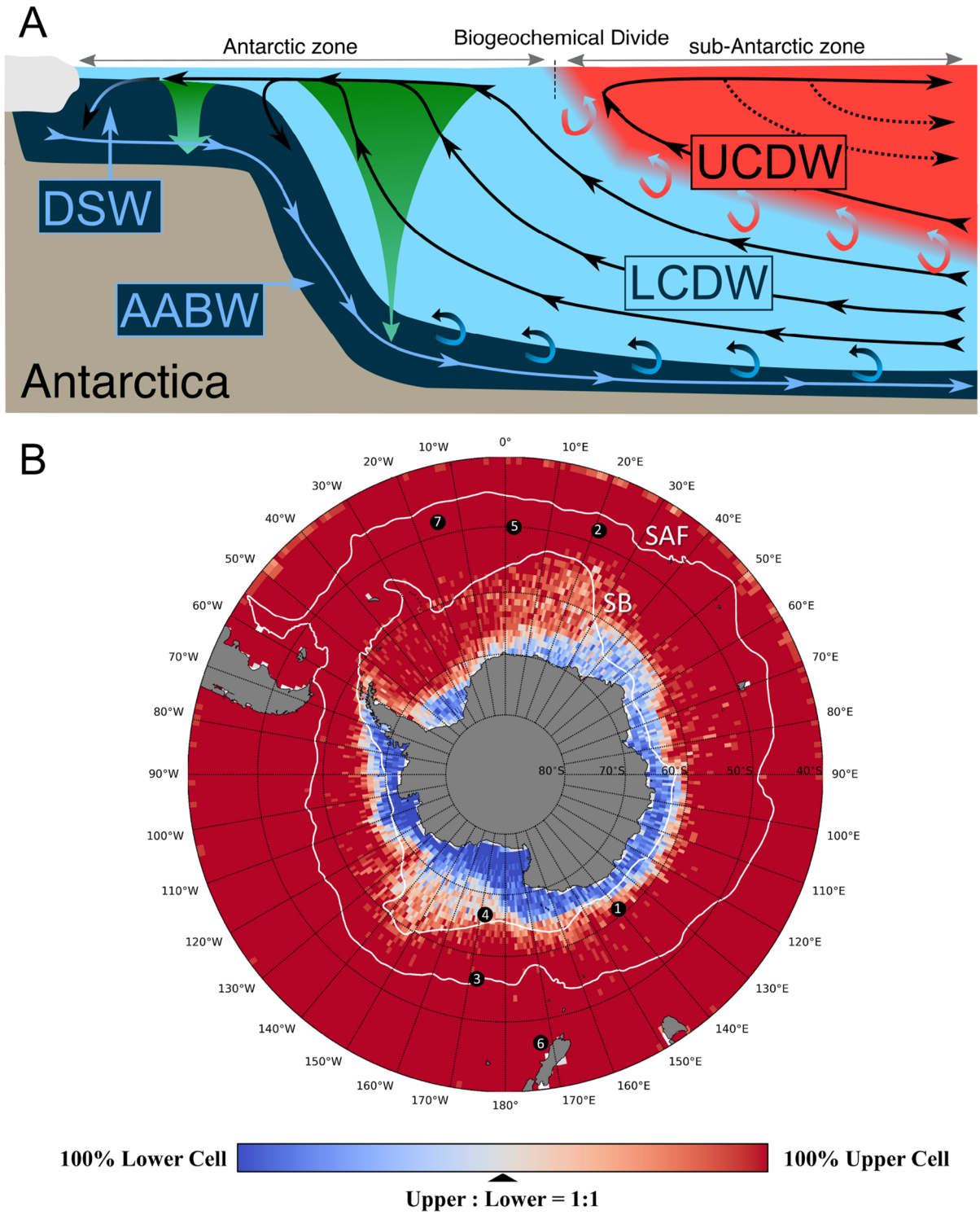

Figure 2. Physical conditions influencing the ocean iron fertilization in the Southern Ocean. (a) Schematic overview of zonal mean major water mass movements showing an upwelling of Upper and Lower Circumpolar Deep Water (UCDW, LCDW), formation of Dense Shelf Water, as well as sinking and northward flow of Antarctic Bottom Water (AABW). The green downward arrows indicate carbon flux attenuation during sinking. Dashed arrows indicate the formation of intermediate and mode waters. The boundary separating the upper and lower overturning cells at the surface marks the Southern Ocean Biogeochemical Divide (SOBD). (b) Map showing the geographical location of the SOBD assessed by virtual particle tracking in a 1/10° physical ocean model ACCESS-OM2-01 (Xie et al., 2022). The southern boundary of the Antarctic Circumpolar Current as well as the Subantarctic Front is also indicated. Points indicate locations of previous meso-scale iron fertilization experiments: 1 = SOIREE, 2 = EisenEX, 3 = SOFeX-N, 4 = SOFeX-S, 5 = EIFEX, 6 = SAGE, 7 = LOHAFEX (Yoon et al., 2018).

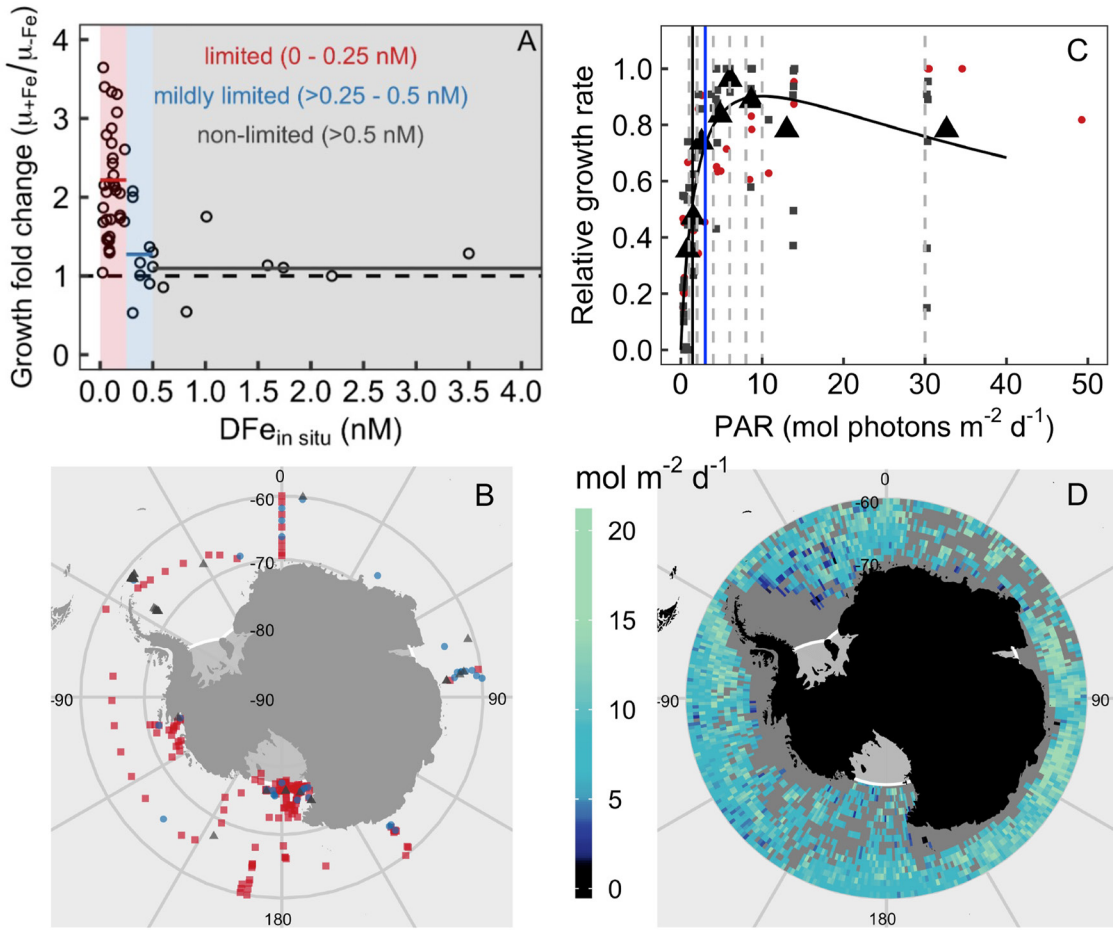

Figure 3. Phytoplankton iron and light limitation in the Southern Ocean. (a) The change in growth rates in DFe-enriched treatments relative to growth rates in the controls (μ_{+Fe}/μ_{-Fe}) is shown as a function of in situ DFe at the locations where the incubated water was collected. The horizontal lines represent the μ_{+Fe}/μ_{-Fe} averages within the defined limitation ranges. (b) Map showing non-limiting (gray triangles), mildly-limiting (blue circles), and limiting (red squares) in situ DFe concentrations during summer (DJF). DFe data was from Tagliabue et al. (2012). (c) Growth versus irradiance curves from experiments with Southern Ocean diatoms (gray squares) and the haptophyte *Phaeocystis antarctica* (red circles). The larger black triangles show averages of all data within a bin (bins separated with vertical dashed lines). The black vertical line at 1.5 mol photons m^{-2} d^{-1} is the irradiance at which the onset of saturation occurs, while the blue vertical line indicates the 3 mol photons m^{-2} d^{-1} threshold for phytoplankton growth determined further north in the Southern Ocean from in situ data (Venables & Moore, 2010). (d) Map showing that the mean mixed layer irradiance (I_{MLD}) is almost everywhere above 1.5 and even 3 mol photons m^{-2} d^{-1} during summer.

3.1.4. Requirement 4: Longer-Term Carbon Storage

The second step in OIF, after the stimulation of CO_2-fixation through fertilization, is the transfer of POC into a water mass that keeps it away from the atmosphere for as long as possible (Robinson et al., 2014). Water masses with such storage potential tend to be in the deep ocean although there are important exceptions (Siegel et al., 2021). There is currently no international legal or political framework that determines how carbon-storage duration (durability) is factored into the formulation of a carbon price, but it is likely that high durability leads to much higher pricing (Ruseva et al., 2020). Hence, carbon transfer into upwelling CDW (low durability) is less favorable than sequestration in AABW (high durability), which is why we focus on the latter in our study (Figure 2a; England, 1995; Robinson et al., 2014; Siegel et al., 2021).

Gravitational sinking of organic particles into the deep ocean is the main pathway considered for the transfer of OIF-derived POC into a water mass enabling high durability (Boyd et al., 2000; Smetacek et al., 2012). In a Monte Carlo approach, we generated 1,000 plausible scenarios for the fraction of primary production reaching any given depth (Figure 4a). This fraction converges toward a narrow range with increasing depth, mostly between 1% and 5% below 1,000 m (Figures 4b–4e). The depth of the upper interface of the AABW is generally between 1,000 and 4,500 m off the Antarctic continental shelf (Figure 4f). Based on the median e-ratio (0.28)

10.1029/2023GB007754

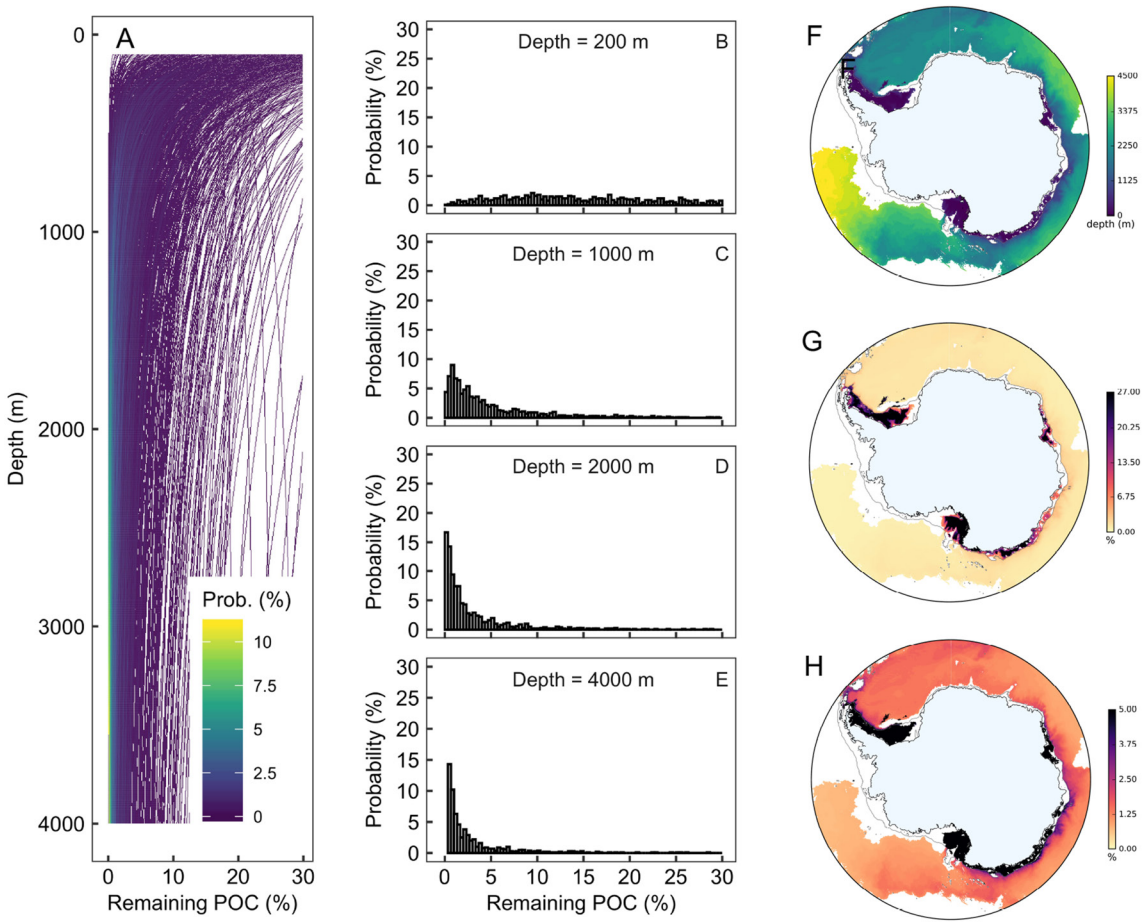

Figure 4. Gravitational ocean iron fertilization (OIF)-mediated particulate organic carbon export. (a) Fraction of primary production reaching depth. Shown are 1,000 profiles based on the Monte Carlo approach. The density color code indicates with what probability the profiles occur in the space of the plot. (b–e) Probabilities of remaining primary production at distinct depth horizons based on the 1,000 profiles. (f) Depth of the upper interface of the Antarctic Bottom Water (AABW) layer. (g) Remaining primary production at the depth of the AABW layer, calculated using the median export-ratio (0.28) and median *b*-value (0.96). Panel (h) the same as in panel (g) but with a narrower scaling to better illustrate differences in the offshore locations.

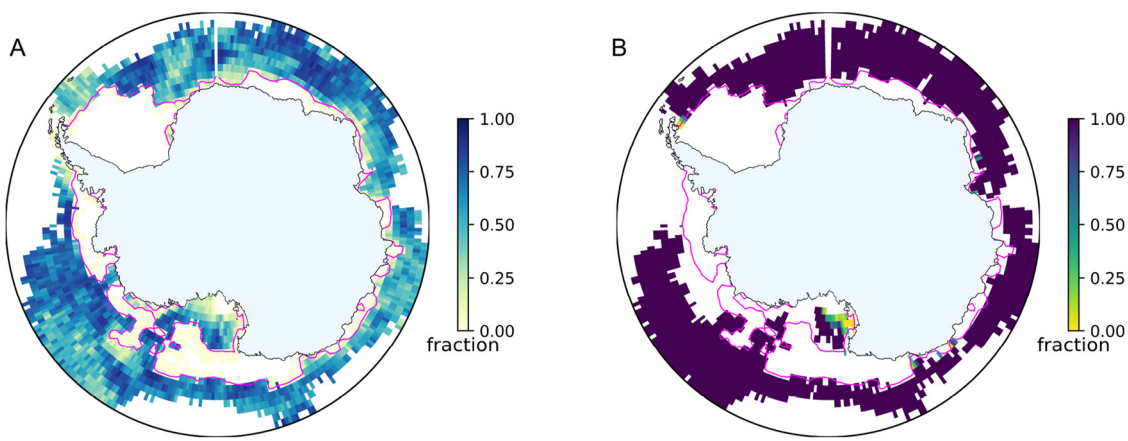

Figure 5. Timescales of air-sea CO_2 exchange estimates. (a) Fraction of CO_2 equilibration (f_{Eq}) for an initial 35 μmol kg^{-1} CO_2 deficit before virtual particles (as equivalents of water masses) leave the surface mixed layer (and therefore contact with the atmosphere). (b) f_{Seq}, which indicates if there is sufficient air-sea CO_2 exchange to match the amount of particulate organic carbon sequestered in AABW. The magenta contours in A and B show the 60% sea ice concentration at the time of particle release (3 January). Sea ice concentrations >60% impeded our analysis so that these regions could not be assessed.

and *b*-value (0.96) (Equation 2), we estimate the percentage of primary production reaching AABW in offshore environments to range between 0.7% and 2.7%, except for some areas near the shelf break (Figure 4g). This range suggests (a) a limited potential to transfer OIF-derived POC from surface water into AABW in offshore regions via sinking, and (b) a ∼four-fold range for sinking POC flux reaching AABW depending on where within the offshore regions OIF is applied.

The potential for downward POC transfer to AABW via gravitational sinking is substantially higher on the Antarctic continental shelves. Here, DSW, the denser precursor feeding into AABW, is formed by surface cooling and brine rejection during sea-ice formation (Ohshima et al., 2013; Williams et al., 2010). DSW occupies relatively shallow depths that can extend to just below the surface mixed layer (Morrison et al., 2020). This means that most, if not all, of the POC that escapes remineralization in surface waters can potentially reach DSW in these continental shelf regions (Figure 4h). As such, DSW serves as a link that physically transports POC from the (near-)surface into AABW, thereby increasing the efficiency of durable CDR (Figure 2a). The problem, however, is that the sub-surface flow of DSW from formation regions to the shelf break is spatially localized on the shelf and occurs in episodic events on timescales of days (Morrison et al., 2020). Thus, OIF-derived POC would have to be entrained into these localized pathways for this shortcut into the deep ocean to work. The exact location where POC sinks is challenging to predict because it takes from days to several weeks following the iron fertilization until downward POC export commences (Boyd et al., 2000; Buesseler et al., 2005; Smetacek et al., 2012). We estimated the regional potential for horizontal displacements of POC for a 1-month period using the virtual particle release experiment and found that neutrally buoyant POC would generally travel <150 km total distance in 1 month in the Weddell and Ross Gyres and on the continental shelves except for larger distances in coastal currents (Figure S3 in Supporting Information S1). These horizontal displacements of POC that occur from the time of fertilization until the onset of POC export must be anticipated for the site selection of the Fe-addition. Hence, OIF on the shelves requires a profound understanding of deep-water formation mechanisms and pathways.

The calculation of gravitational POC transfer efficiency from the surface into the AABW is based on mean export-ratios and *b*-values published for the Southern Ocean (Tables S4 and S5 in Supporting Information S1), with large variability based on a wide range of observations (Figure 4). Consistent with observations, mesoscale OIF experiments in the Southern Ocean have found variable responses of downward POC export to fertilization. Some observations suggest a comparable export to naturally-occurring blooms (Buesseler et al., 2005), while another study reports extremely efficient export (Smetacek et al., 2012). Two studies found no noticeable increase in export, although this was arguably because observations stopped before the export commenced (Boyd et al., 2000; Smetacek et al., 2012). POC transfer efficiency has frequently been shown to be controlled by the pelagic community structure (Assmy et al., 2013; Boyd & Newton, 1995; Guidi et al., 2009; Wassmann, 1998). Hence, it could be argued that targeting "transfer-efficient" communities for OIF, or even seeding them alongside OIF operations, could optimize e-ratios and *b*-values and lead to more POC sequestration than Figure 4 suggests. For example, fertilizing phytoplankton communities with abundant *Phaeocystis antarctica* may increase carbon sequestration compared to fertilized diatom communities due to *Phaeocystis*' inherently higher Carbon to nutrient ratio (Arrigo et al., 1999). However, our ability to predict the POC transfer efficiency based on the plankton community composition is poor (Burd et al., 2016), suggesting that such optimization is unlikely to be successful with our current level of understanding (and the seeding of phytoplankton communities seems unlikely to receive social license and/or legal allowance). Furthermore, phytoplankton communities that result in high transfer-efficiencies may not prevail in a target region during the short period in summer where conditions enable OIF (Arrigo & Tagliabue, 2005). In light of these limitations, it seems justifiable to base our estimates of POC transfer to AABW on a wide range of observations and thus to accept that the CDR efficiency of OIF is currently rather unpredictable within the estimated bounds. Due to these arguments, the transfer efficiency of OIF-derived POC into AABW has a profound influence on the analysis of (cost-)efficiency.

3.1.5. Requirement 5: Air-Sea CO_2 Equilibration

The third step in OIF, after C-fixation and carbon export to deep waters, is the transfer of atmospheric CO_2 into the ocean (Gnanadesikan & Marinov, 2008). We employed a "bucket" approach to estimate what fraction of a water parcel with a seawater CO_2 deficit (induced by OIF) would be replenished with atmospheric CO_2 before the water parcel was subducted (i.e., f_{Eq} as defined in Section 2.3). The approach has some strengths and weaknesses which need to be highlighted before discussing the outcome of the calculations. Strengths are (a) comparing the OIF with the no-OIF scenario accounts for "expected" background changes in DIC from ocean

processes including vertical transport, eddy mixing and storm mixing that are reflected in observations. This leads to a more realistic representation of air-sea CO_2 exchange, since natural variability is considered in the calculation. (b) Using Lagrangian particles to trace water parcels enables us to link f_{Eq} with the origin of the OIF patch. This provides a gridded data set which is crucial for the spatially resolved OIF (cost-)efficiency analysis, the key novelty of the study (Sections 3.3 and 3.4). (c) Lagrangian particle tracking is computationally relatively inexpensive, enabling the use of high-resolution model output. This is critical for improved representation of deep-water formation (Heuzé, 2021). Weaknesses are (a) the approach neglects patch dilution, which reduces air-sea pCO_2 gradients in the fertilized patch but increases the surface area for CO_2 exchange with the atmosphere. These are opposing effects on air-sea CO_2 exchange and we are unable to quantify their relative influence. (b) Patch dilution can also increase productivity (Lehahn et al., 2017) so that an initial DIC deficit of 35 µmol/kg may increase over time. This is not accounted for in our calculations. (c) The assumption that influx is terminated upon the subduction of a water parcel (Figure 1) is simplistic since a parcel could resurface after its subduction and CO_2 influx could continue. (d) The simulation assumes an initial DIC deficit in the surface mixed-layer and would not be applicable for potential OIF-induced DIC deficits generated below the mixed-layer. Despite these weaknesses, our approach seems to provide a useful overview of where in the Southern Ocean limitations on OIF set by air-sea CO_2 exchange could become problematic. As described in the next paragraph, air-sea CO_2 exchange was estimated to only limit OIF (cost-)efficiency in a few AABW formation regions on the shelves. This is qualitatively similar to previous findings (Arrigo & Tagliabue, 2005; Gnanadesikan & Marinov, 2008) and provides some confidence that our estimates are reasonable.

The calculations suggest that f_{Eq} is generally >50% off the continental shelves (Figure 5a). Figure 5b shows that this degree of re-equilibration with atmospheric CO_2 is several-fold more than needed to equilibrate the amount of CO_2 sequestered in AABW off the shelves (i.e., $f_{Seq} \geq 1$, or ≥100% as shown in Figure 5b). Accordingly, air-sea CO_2 influx is unlikely to constrain the efficiency of OIF in the open Southern Ocean, at least in areas where the limited extent of sea ice allows this type of analytical approach.

In contrast, air-sea CO_2 influx can limit OIF efficiency in some parts of the Antarctic shelf, most noticeably in the Ross Sea where $f_{Seq} < 1$ near the coast (Figure 5b). This result is broadly consistent with a regional model that also identified air-sea CO_2 influx as a potential limitation of OIF in the area (Arrigo & Tagliabue, 2005). On other shelf areas, there are only some scattered locations around Eastern Antarctica and at the tip of the Antarctic Peninsula where air-sea CO_2 influx is not sufficient to match the amount of POC sequestered in AABW (Figure 4b). The reasons for the insufficiency in these regions are twofold. First, the identified shelf regions are relatively efficient in transferring POC from the surface to AABW because AABW (or DSW as its precursor) can be present at shallow depths (Figure 4f). Thus, relatively high amounts of POC are sequestered in AABW (Figure 4g) so that more atmospheric CO_2 influx is needed to match the amount of sequestered POC. Second, AABW can form in the identified regions shortly after the simulated OIF operation in January so that water parcels have short residence times in the surface, thereby restricting the time for air-sea CO_2 influx. Due to these constraining factors, air-sea CO_2 influx is considered in the analysis of (cost-)efficiency.

3.2. Spatial Patterns of CDR (Cost-)Efficiency

The spatial analysis of CDR (t CO_2 km^{-2}) and associated costs (US$ t^{-1} CO_2) reveals pronounced regional differences in both parameters (Figure 6). The most favorable conditions are found on or very close to Antarctic shelves where AABW or its precursors are relatively shallow (Figures 2a and 3f). In the Ross Sea, for example, >2 t CO_2 km^{-2} can be sequestered at a cost much below 100 US$ t^{-1} $CO_2{}^{-1}$. However, limited air-sea CO_2 influx can still reduce CDR and increase the costs in the Ross Sea near the coast (Figure 6). Similarly, (cost-)efficient conditions can be found at the tip of the Antarctic Peninsula, Prydz Bay, and a few smaller spots on the coast of Eastern Antarctica (Figure 6). In contrast, CDR declines and costs rise sharply further offshore in the open Southern Ocean. Here, CDR are largely below 0 t CO_2 km^{-2} (gray areas in Figure 6a) because the emissions associated with iron delivery and N_2O-related offsets are higher than CDR.

There are several limitations in the spatial analysis of CDR (cost-)efficiency. First, relatively large data gaps are present throughout the study region due to the influence of sea-ice on the analysis of air-sea CO_2 transfer (Figure 5). Thus, particularly (cost-)efficient or inefficient regions may have been missed. Second, one requirement for our analysis is that OIF would be restricted to the south of the SOBD to limit offsets in (cost-)efficiency due to nutrient robbing (Section 3.1.1). However, our spatial analysis partially extends to regions north of the

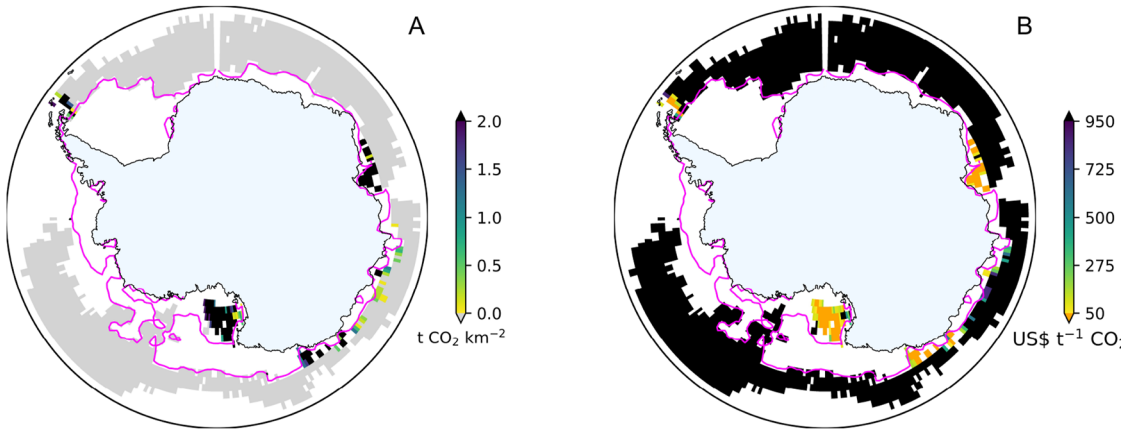

Figure 6. The magnitude of CDR and associated costs. (a) CDR achieved south of 60°S as calculated using Equation 5 using median e-ratio and *b*-value to calculate flux attenuation. (b) Costs per t CO_2 sequestered. Values were calculated by dividing an intermediate $costs_{area}$ estimate for ocean iron Fertilization (74 $US km^{-2}, Table S6 in Supporting Information S1) by CDR from (a) as in Equation 11.

SOBD (compare Figures 2b and 6). Here, CDR efficiency would further decline (costs would increase) when accounting for the reduction of downstream productivity due to nutrient robbing. We have not factored this offset into Equation 5 because the complicated global ocean teleconnections between nutrient drawdown in the Southern Ocean and nutrient availability outside the Southern Ocean make it difficult to constrain (Hauck et al., 2018). Third, our cost-calculation does not account for purchasing or chartering a ship but considers a "ship of opportunity scenario" that has multiple tasks and can carry out OIF opportunistically during the Southern Ocean productivity season. Likewise, costs to gain legal permission for OIF or to measure, report, or verify CDR were also not considered in the calculations as we are unable to constrain them. Assuming these factors would double the operational costs (Equation 10), it would double the costs per tonne CO_2 at any given location in Figure 6b. Fourth, we defined that POC sequestration in upwelling Southern Ocean water masses like CDW would have no value because these re-expose respired CO_2 to the surface within decades (Robinson et al., 2014; Siegel et al., 2021; Tamsitt et al., 2017). Instead, we defined that POC sequestration in AABW has maximum value as it locks POC in the deep-ocean for much longer timescales (Siegel et al., 2021). This categorization was necessary because we were unable to link sequestration timescale to every depth and location where OIF-derived organic carbon is potentially respired. In reality, however, longer-term POC storage is certainly more valuable than short-term storage, but short-term storage is not worthless (Ruseva et al., 2020). Concepts to rate the amount of sequestered carbon with its sequestration longevity (e.g., "ton-year accounting"; Chay et al., 2022) may make short-term CDR more valuable off the shelves than the maps shown in Figure 6 suggest. Thus, it needs to be kept in mind that our analysis of (cost-)efficiency leads to results that are valid under the assumptions made here but could be modified when a more sophisticated carbon accounting methodology is applied.

3.3. Variability in OIF (Cost-)Efficiency

We used a Monte Carlo approach to estimate the likelihood distributions for longer-term CDR (defined above as POC transfer into AABW) for two different AABW depths (200 and 1,000 m) and for complete or incomplete CO_2 equilibration (f_{Seq} = 0.5 or 1). These two conditions encompass the most relevant parameter range for an on-the-shelf (200 m, 0.5) and off-the-shelf (1,000 m, 1) scenario (Figure 7).

Simulated variability in either f_{N_2O} or $O_{transport}$ had a small influence on CDR variability in all of the scenarios (Figures 7a and 7b). Simulated variability in C/Fe had a larger influence on CDR variability but only for the 200 m scenario (Figures 7a and 7b). Simulated variability in POC_{AABW} had by far the largest influence on CDR variability in all scenarios considered here (hence constraining the factors that control export flux attenuation offers the greatest potential for improving the predictability of CDR as has been discussed in Section 3.1.4). Unsurprisingly, CDR variability is highest when simulating variability in all four components (f_{N_2O}, $O_{transport}$, C/Fe, and POC_{AABW}) simultaneously. The variability in costs is shown as histograms in Figures 7c and 7d. Here, turquoise and red histograms show cost distributions for an AABW surface depth of 200 and 1,000 m respectively. The simulations shown in Figure 7c assume that f_{Seq} = 1, that is, that all CO_2 sequestered from seawater is

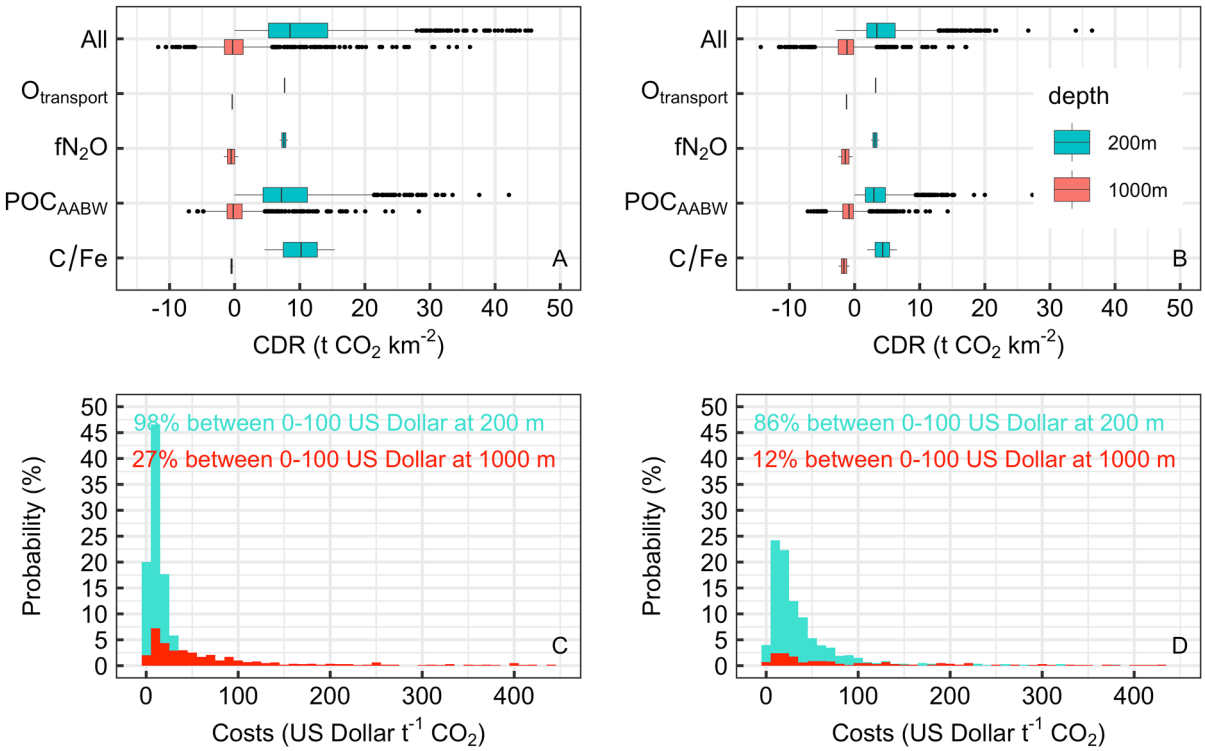

Figure 7. Variability in the (cost-)efficiency of ocean iron fertilization (OIF). (a) Results from the Monte Carlo simulations (n = 1,000) where individual components of Equation 5 were varied within their data-constrained ranges to assess their influence on CDR variability. Boxplots show the median, 25% and 75% percentiles (boxes), minimum/maximum (whiskers), and outliers (dots). Turquoise and red boxes are scenarios where the Antarctic Bottom Water (AABW) surface layer is at 200 and 1,000 m, respectively. f_{Seq} was set to 1 in these calculations, meaning that air-sea CO_2 influx puts no constraints on the CDR. Panel (b) same as in panel (a) but assuming f_{Seq} = 0.5. (c) Histogram of OIF costs in scenarios where the AABW surface layer is at 200 m (red) or 1,000 m (turquoise), respectively and f_{Seq} = 1. (d) Same as in (c) but with f_{Seq} = 0.5.

matched with the influx of atmospheric CO_2. In this case, there is a 98% probability that costs will be between 0 and 100 US$ t^{-1} CO_2^{-1} when AABW is only 200 m deep. However, the probability of being in this price range is only 27% when AABW is at 1,000 m, and there is a 58% chance that the costs are negative, meaning that OIF generated more CO_2 equivalents through shipping emissions and N_2O generation than it sequestered (Figure 7c). Cost distributions become less favorable under the assumption that only half of the CO_2 sequestered from seawater is matched by atmospheric CO_2 influx (i.e., f_{Seq} = 0.5; Figure 7d), a scenario that can occur in some shelf regions (Figure 5b). Here, costs are only between 0 and 100 US$ t^{-1} CO_2^{-1} in 86% (AABW at 200 m) and 12% (AABW at 1,000 m) of the cases. Negative costs still hardly occur for the 200 m AABW scenario (0.6% of cases) but predominate for the 1,000 m AABW scenario (80% of cases).

An important takeaway from the assessment of variability is that CDR is negative in the majority of cases when AABW is deeper than 1,000 m. Thus, although there is still a chance that CDR is (cost-)efficient under circumstances where, the likelihood for this is low (Section 3.1.4). Accordingly, there is a high risk of failed OIF over large parts of the open Southern Ocean where the AABW is deeper than 1,000 m (Figure 4f). The variability of OIF (cost-)efficiency is also considerable when AABW occurs at 200 m depth (possible in some shelf regions, Figure 4f). However, costs are in most cases between only 0–100 US$ t^{-1} CO_2^{-1}. Any costs within this range are low compared to other CDR methods (Fuss et al., 2018) and are therefore potentially attractive from an economic standpoint. Nevertheless, the unpredictability of costs, even within this low range, remains a challenge since carbon markets may demand more predictable CDR and costs.

3.4. Environmental and Legal Ramifications

For OIF to move forward, CDR benefits (as well as environmental side-effects not considered in this study) would need to be re-evaluated within at least four partially overlapping layers of international and domestic law

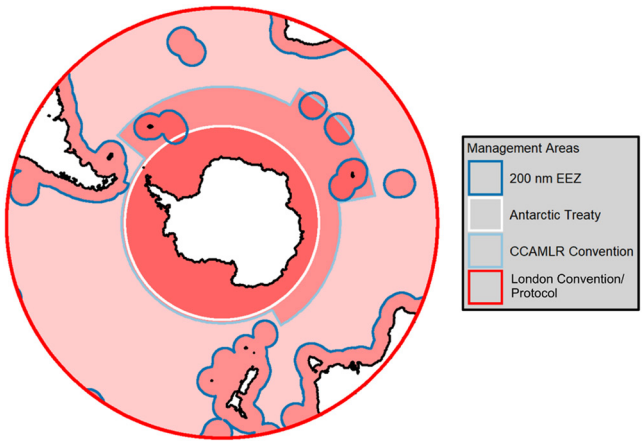

Figure 8. Legal constraints on ocean iron fertilization in the Southern Ocean. The map shows four layers of international or domestic law around Antarctica and Sub-Antarctic islands. Each layer is shaded in red with an overlapping law leading to a darker red color. The London Convention and London Protocol apply globally. National law applies within the exclusive economic zones of states, including the sub-Antarctic islands. Commission for the Conservation of Antarctic Marine Living Resources governs marine living resources in sectors around Antarctica. The Antarctic Treaty applies south of 60°S.

(Figure 8). The 1991 Madrid Protocol to the Antarctic Treaty (covering the area south of 60°S) commits to "comprehensive protection of the Antarctic environment and dependent and associated ecosystems". The Ross Sea, which we identify as a cost-efficient region for OIF (Figure 6), is the location of a marine protected area formed under the Commission for the Conservation of Antarctic Marine Living Resources (CCAMLR), so it may be very difficult for OIF to proceed there. More concrete rules apply to member states of the 1972 London Convention (LC) on Marine Pollution (currently 87) and the 1996 London Protocol (LP) (currently 53). Both of these treaties regulate ocean dumping of waste in the ocean. If OIF activities are only for "legitimate scientific research" they are not considered "dumping." However, once OIF activities upscale beyond legitimate scientific research, the position under the two treaties diverges. The LC would likely allow its member states to issue a permit for OIF, while OIF would likely be prohibited for member states in the LP. The environmental and legal ramifications underscore the wide-ranging challenges of OIF, which go far beyond resolving open questions in physical, chemical, and biological oceanography.

4. Conclusions

The analysis presented here considers different biogeochemical variables that affect the CDR efficiency of OIF. These variables were assessed consecutively and finally synthesized into spatially resolved costs per tonne CO_2 removed. The focus on (cost-)efficiency was motivated by the notion that the implementation of different CDR methods is more likely driven by their (cost-)efficiency than their maximum CDR capacity in the Earth system (Bellamy & Geden, 2019; Rickels et al., 2012). The approach chosen here to evaluate spatially resolved (cost-)efficiency in the Southern Ocean has several limitations and required assumptions on how future carbon accounting may function. For example, there may be other biogeochemical factors not considered here (e.g., DOC) that could modify the (cost-)efficiency. However, the framework allows updating and can thus be adapted and improved over time.

The analysis of variability in (cost-)efficiency underlines that one key challenge for OIF remains the predictability of CDR, consistent with conclusions made from the first era of OIF in situ experiments during the 1990s and early 2000s (Boyd et al., 2007; de Baar et al., 2005; Yoon et al., 2018). OIF will only become a credible method if the amounts of CDR can be accounted for accurately and with a precision that satisfies widely agreed accounting criteria which have yet to be developed (Arcusa & Sprenkle-Hyppolite, 2022). It is questionable whether the level of variability assessed here, spanning several orders of magnitude (Figure 6), will satisfy future accounting standards. Thus, progressing OIF requires drastically improved understanding of the factors modulating CDR (i.e., primarily flux attenuation, see Section 3.1.4) or requires the ability to precisely determine these factors empirically for individual OIF deployments.

Our multi-facetted analysis is timely as there is renewed interest in OIF for large-scale CDR operations. A recent review by the National Academy of Sciences Engineering and Medicine (NASEM) concluded that substantially more research is needed to fully assess OIF and called for 290 million US$ within 10 years (NASEM, 2021). Indeed, there are already emerging efforts to explore new ideas for OIF implementation and establish OIF field research (Buesseler et al., 2023; Emerson, 2019; Oeste et al., 2017; Yoon et al., 2018). Although our informed back-of-the-envelope approach is less internally consistent than biogeochemical modeling, it enabled critically important guidance for these emerging efforts by mapping (cost-)efficiency for OIF south of 60°S. Such insights are currently difficult to obtain from biogeochemical models due to computational constraints and their limitations in reproducing AABW pathways (Section 2.1). We found relatively pronounced gradients in OIF (cost-)efficiency, suggesting that any iron fertilizer would require precise injection to maximize OIF efficiency. This finding argues against recent suggestions to distribute iron through atmospheric transport (Emerson, 2019; Oeste et al., 2017) since it seems unlikely that high precision would be achievable by such means.

Buesseler et al. (2023) and Yoon et al. (2018) have proposed potential OIF locations in the Southern Ocean based on nutrient conditions and considered much of the Southern Ocean area for future OIF research, including the

open Southern Ocean. Our findings on (cost-)efficiency provide little incentive to further explore OIF in the open Southern Ocean south of 60°S. (Cost-)efficient OIF in these regions would require that OIF predictably generates very efficient POC transfer to great depth, as has been observed only in one study so far (Smetacek et al., 2012). (But note that even efficient POC transfer would not solve the problem of "nutrient robbing" north of the biogeochemical divide discussed in Section 3.1.1). Although we find such highly (cost-)efficient cases for open ocean regions also within the variability determined here, they are the exception rather than the rule (Figure 7). In contrast, our analysis provides an argument to further explore the concept of OIF in some Antarctic shelf regions. However, even if future research confirmed a high (cost-)efficiency on Antarctic shelves, up-scaling beyond scientific research seems unlikely in the near future due to international treaties (Section 3.4) and public perceptions (Cox et al., 2021). Thus, the benefit of shelf OIF with its potentially high (cost-)efficiency would have to be carefully evaluated against its environmental implications.

Data Availability Statement

The Lagrangian particle trajectory output used in this analysis and the derived data can be found as Bach et al. (2021) under the DOI: https://doi.org/10.5281/zenodo.5576833.

Acknowledgments
The authors thank Argo, the NOAA National Sea Ice Data Center, the National Centers for Environmental Information and Remote Sensing Systems, and NASA Giovanni for openly providing the climatological data used in this study. We also thank Alessandro Tagliabue for kindly providing the dissolved iron data. Argo data were collected and made freely available by the International Argo Program and the national programs that contribute to it (http://www.argo.ucsd.edu; http://argo.jcommops.org; http://doi.org/10.17882/42182). The Argo Program is part of the Global Ocean Observing System. NASA Giovanni is developed and maintained by the NASA GES DISC. We acknowledge the mission scientists and Principal Investigators who provided the data. We also thank three excellent reviewers and the editor for their thoughtful and constructive comments.

References

Arcusa, S., & Sprenkle-Hyppolite, S. (2022). Snapshot of the carbon dioxide removal certification and standards ecosystem (2021–2022). *Climate Policy*, *22*(9–10), 1–14. https://doi.org/10.1080/14693062.2022.2094308

Arrigo, K. R., Robinson, D. H., Worthen, D. L., Dunbar, R. B., DiTullio, G. R., VanWoert, M., & Lizotte, M. P. (1999). Phytoplankton community structure and the drawdown of nutrients and CO_2 in the Southern Ocean. *Science*, *283*(5400), 365–367. https://doi.org/10.1126/science.283.5400.365

Arrigo, K. R., & Tagliabue, A. (2005). Iron in the Ross Sea: 2. Impact of discrete iron addition strategies. *Journal of Geophysical Research-Part C Oceans*, *110*(C3), 1–16. https://doi.org/10.1029/2004JC002568

Assmy, P., Smetacek, V., Montresor, M., Klaas, C., Henjes, J., Strass, V. H., et al. (2013). Thick-shelled, grazer-protected diatoms decouple ocean carbon and silicon cycles in the iron-limited Antarctic Circumpolar Current. *Proceedings of the National Academy of Sciences*, *110*(51), 20633–20638. https://doi.org/10.1073/pnas.1309345110

Aumont, O., & Bopp, L. (2006). Globalizing results from ocean in situ iron fertilization studies. *Global Biogeochemical Cycles*, *20*(2), 1–15. https://doi.org/10.1029/2005GB002591

Bach, L. T., Ho, D. T., Boyd, P. W., & Tyka, M. D. (2023). Toward a consensus framework to evaluate air–sea CO_2 equilibration for marine CO_2 removal. *Limnology and Oceanography Letters*, *8*, 685–691. https://doi.org/10.1002/lol2.10330

Bach, L. T., Tamsitt, V., Baldry, K., McGee, J., Laurenceau-Cornec, E. C., Strzepek, R. F., et al. (2021). Trajectories and metadata for Bach et al.: "Holistic re-evaluation of Southern Ocean Iron Fertilization for atmospheric CO2 removal" [Dataset]. Zenodo. https://doi.org/10.5281/zenodo.5576833

Bellamy, R., & Geden, O. (2019). Govern CO_2 removal from the ground up. *Nature Geoscience*, *12*(11), 874–876. https://doi.org/10.1038/s41561-019-0475-7

Bowie, A. R., Maldonado, M. T., Frew, R. D., Croot, P. L., Achterberg, E. P., Mantoura, R. C., et al. (2001). The fate of added iron during a mesoscale fertilisation experiment in the Southern Ocean. *Deep Sea Research Part II: Topical Studies in Oceanography*, *48*(11–12), 2703–2743. https://doi.org/10.1016/S0967-0645(01)00015-7

Boyd, P., & Newton, P. (1995). Evidence of the potential influence of planktonic community structure on the interannual variability of particulate organic carbon flux. *Deep-Sea Research Part I Oceanographic Research Papers*, *42*(5), 619–639. https://doi.org/10.1016/0967-0637(95)00017-z

Boyd, P. W., & Abraham, E. R. (2001). Iron-mediated changes in phytoplankton photosynthetic competence during SOIREE. *Deep Sea Research Part II: Topical Studies in Oceanography*, *48*(11–12), 2529–2550. https://doi.org/10.1016/S0967-0645(01)00007-8

Boyd, P. W., Jickells, T., Law, C. S., Blain, S., Boyle, E. A., Buesseler, K. O., et al. (2007). Mesoscale iron enrichment experiments 1993–2005: Synthesis and future directions. *Science*, *315*(5812), 612–617. https://doi.org/10.1126/science.1131669

Boyd, P. W., Law, C. S., Wong, C. S., Nojiri, Y., Tsuda, A., Levasseur, M., et al. (2004). The decline and fate of an iron-induced subarctic phytoplankton bloom. *Nature*, *428*(6982), 549–553. https://doi.org/10.1038/nature02437

Boyd, P. W., Watson, A. J., Law, C. S., Abraham, E. R., Trull, T., Murdoch, R., et al. (2000). A mesoscale phytoplankton bloom in the polar Southern Ocean stimulated by iron fertilization. *Nature*, *407*(6805), 695–702. https://doi.org/10.1038/35037500

Buesseler, K. O. (2012). The great iron dump. *Nature*, *487*(7407), 305–306. https://doi.org/10.1038/487305a

Buesseler, K. O., Andrews, J. E., Pike, S. M., Charette, M. A., Goldson, L. E., Brzezinski, M. A., & Lance, V. P. (2005). Particle export during the southern Ocean Iron experiment (SOFeX). *Limnology & Oceanography*, *50*(1), 311–327. https://doi.org/10.4319/lo.2005.50.1.0311

Buesseler, K. O., Chai, F., Karl, D., Ramakrishna, K., Satterfield, T., Siegel, D., et al. (2023). Ocean iron fertilization: Assessing its potential as a climate solution.

Burd, A. B., Buchan, A., Church, M., Landry, M., McDonnell, A., Passow, U., et al. (2016). Towards a transformative understanding of the ocean s biological pump: Priorities for future research.

Chay, F., Badgley, G., Martin, K., Freeman, J., Hamman, J., & Cullenward, D. (2022). Unpacking ton-year accounting.

Cox, E., Boettcher, M., Spence, E., & Bellamy, R. (2021). Casting a wider net on ocean NETs. *Frontiers in Climate*, *3*, 576294. https://doi.org/10.3389/fclim.2021.576294

de Baar, H. J. W., Boyd, P. W., Coale, K. H., Landry, M. R., Tsuda, A., Assmy, P., et al. (2005). Synthesis of iron fertilization experiments: From the iron age in the age of enlightenment. *Journal of Geophysical Research: Oceans*, *110*(C9), 1–24. https://doi.org/10.1029/2004JC002601

Eilers, P. H. C., & Peeters, J. C. H. (1988). A model for the relationship between light intensity and the rate of photosynthesis in phytoplankton. *Ecological Modelling*, *42*(3–4), 199–215. https://doi.org/10.1016/0304-3800(88)90057-9

Emerson, D. (2019). Biogenic iron dust: A novel approach to ocean iron fertilization as a means of large scale removal of carbon dioxide from the atmosphere. *Frontiers in Marine Science*, *6*, 1–8. https://doi.org/10.3389/fmars.2019.00022

England, M. H. (1995). The age of water and ventilation timescales in a global ocean model. *Journal of Physical Oceanography*, *25*(11), 2756–2777. https://doi.org/10.1175/1520-0485(1995)025<2756:TAOWAV>2.0.CO;2

Fu, W., & Wang, W. L. (2022). Biogeochemical equilibrium responses to maximal productivity in high nutrient low chlorophyll regions. *Journal of Geophysical Research: Biogeosciences*, *127*(5), 1–13. https://doi.org/10.1029/2021JG006636

Fuss, S., Lamb, W. F., Callaghan, M. W., Hilaire, J., Creutzig, F., Amann, T., et al. (2018). Negative emissions—Part 2: Costs, potentials and side effects. *Environmental Research Letters*, *12*(6), 063002. https://doi.org/10.1088/1748-9326/aabf9f

Gattuso, J.-P., Magnan, A. K., Bopp, L., Cheung, W. W. L., Duarte, C. M., Hinkel, J., et al. (2018). Ocean solutions to address climate change and its effects on marine ecosystems. *Frontiers in Marine Science*, *5*, 337. https://doi.org/10.3389/fmars.2018.00337

Gnanadesikan, A., & Marinov, I. (2008). Export is not enough: Nutrient cycling and carbon sequestration. *Marine Ecology Progress Series*, *364*, 289–294. https://doi.org/10.3354/meps07550

Gnanadesikan, A., Sarmiento, J. L., & Slater, R. D. (2003). Effects of patchy ocean fertilization on atmospheric carbon dioxide and biological production. *Global Biogeochemical Cycles*, *17*(2), 1–17. https://doi.org/10.1029/2002gb001940

Griffies, S. M. (2012). Elements of the Modular Ocean Model (MOM) 2012 release with updates. Retrieved from https://mom-ocean.github.io/assets/pdfs/MOM5_manual.pdf

Guidi, L., Stemmann, L., Jackson, G. A., Ibanez, F., Claustre, H., Legendre, L., et al. (2009). Effects of phytoplankton community on production, size and export of large aggregates: A world-ocean analysis. *Limnology & Oceanography*, *54*(6), 1951–1963. https://doi.org/10.4319/lo.2009.54.6.1951

Harrison, D. P. (2013). A method for estimating the cost to sequester carbon dioxide by delivering iron to the ocean. *International Journal of Global Warming*, *5*(3), 231–254. https://doi.org/10.1504/IJGW.2013.055360

Hauck, J., Lenton, A., Langlais, C., & Matear, R. (2018). The fate of carbon and nutrients exported out of the Southern Ocean. *Global Biogeochemical Cycles*, *32*(10), 1556–1573. https://doi.org/10.1029/2018GB005977

He, J., & Tyka, M. D. (2023). Limits and CO_2 equilibration of near-coast alkalinity enhancement. *Biogeosciences*, *20*(1), 27–43. https://doi.org/10.5194/bg-20-27-2023

Heuzé, C. (2021). Antarctic bottom water and north Atlantic deep water in CMIP6 models. *Ocean Science*, *17*(1), 59–90. https://doi.org/10.5194/os-17-59-2021

Holte, J., Talley, L. D., Gilson, J., & Roemmich, D. (2017). An Argo mixed layer climatology and database. *Geophysical Research Letters*, *44*(11), 5618–5626. https://doi.org/10.1002/2017GL073426

Huang, Y., Tagliabue, A., & Cassar, N. (2022). Data-driven modeling of dissolved iron in the global ocean. *Frontiers in Marine Science*, *9*, 1–14. https://doi.org/10.3389/fmars.2022.837183

Ito, T., & Follows, M. J. (2005). Preformed phosphate, soft tissue pump and atmospheric CO_2. *Journal of Marine Research*, *63*(4), 813–839. https://doi.org/10.1357/0022240054663231

Jin, X., & Gruber, N. (2003). Offsetting the radiative benefit of ocean iron fertilization by enhancing N_2O emissions. *Geophysical Research Letters*, *30*(24), 1–4. https://doi.org/10.1029/2003GL018458

Krishnamurthy, A., Moore, J. K., & Doney, S. C. (2008). The effects of dilution and mixed layer depth on deliberate ocean iron fertilization: 1-D simulations of the southern ocean iron experiment (SOFeX). *Journal of Marine Systems*, *71*(1–2), 112–130. https://doi.org/10.1016/j.jmarsys.2007.07.002

Large, W. G., & Yeager, S. G. (2009). The global climatology of an interannually varying air-sea flux data set. *Climate Dynamics*, *33*(2–3), 341–364. https://doi.org/10.1007/s00382-008-0441-3

Laurenceau-Cornec, E. C., Mongin, M., Trull, T. W., Bressac, M., Cavan, E. L., Bach, L. T., et al. (2023). Concepts toward a global mechanistic mapping of ocean carbon export. *Global Biogeochemical Cycles*, *37*(9), e2023GB007742. https://doi.org/10.1029/2023GB007742

Law, C. S., & Ling, R. D. (2001). Nitrous oxide flux and response to increased iron availability in the Antarctic Circumpolar Current. *Deep Sea Research Part II: Topical Studies in Oceanography*, *48*(11–12), 2509–2527. https://doi.org/10.1016/S0967-0645(01)00006-6

Lehahn, Y., Koren, I., Sharoni, S., D'Ovidio, F., Vardi, A., & Boss, E. (2017). Dispersion/dilution enhances phytoplankton blooms in low-nutrient waters. *Nature Communications*, *8*, 1–8. https://doi.org/10.1038/ncomms14868

Marinov, I., Gnanadesikan, A., Toggweiler, J. R., & Sarmiento, J. L. (2006). The Southern Ocean biogeochemical divide. *Nature*, *441*(7096), 964–967. https://doi.org/10.1038/nature04883

Martin, J. H. (1990). Glacial-interglacial CO_2 change: The iron hypothesis. *Paleoceanography*, *5*, 1–13. https://doi.org/10.1029/pa005i001p00001

Martin, J. H., Knauer, G. A., Karl, D. M., & Broenkow, W. W. (1987). VERTEX: Carbon cycling in the northeast Pacific. *Deep-Sea Research Part A: Oceanographic Research Papers*, *34*(2), 267–285. https://doi.org/10.1016/0198-0149(87)90086-0

Martínez-García, A., Sigman, D. M., Ren, H., Anderson, R. F., Straub, M., Hodell, D. A., et al. (2014). Iron fertilization of the subantarctic ocean during the last ice age. *Science*, *343*(6177), 1347–1350. https://doi.org/10.1126/science.1246848

Moorman, R., Morrison, A. K., & Hogg, A. M. C. (2020). Thermal responses to Antarctic ice shelf melt in an eddy-rich Global Ocean-Sea Ice model. *Journal of Climate*, *33*(15), 6599–6620. https://doi.org/10.1175/JCLI-D-19-0846.1

Morrison, A. K., Hogg, A. M., England, M. H., & Spence, P. (2020). Warm Circumpolar Deep Water transport toward Antarctica driven by local dense water export in canyons. *Science Advance*, *6*(18), eaav2516. https://doi.org/10.1126/sciadv.aav2516

NASEM. (2021). *A research strategy for ocean-based carbon dioxide removal and sequestration*. Doney.

Nemet, G. F., Callaghan, M. W., Creutzig, F., Fuss, S., Hartmann, J., Hilaire, J., et al. (2018). Negative emissions—Part 3: Innovation and upscaling. *Environmental Research Letters*, *13*(6), 06300. https://doi.org/10.1088/1748-9326/aabff4

Oeste, F. D., De Richter, R., Ming, T., & Caillol, S. (2017). Climate engineering by mimicking natural dust climate control: The iron salt aerosol method. *Earth System Dynamics*, *8*, 1–54. https://doi.org/10.5194/esd-8-1-2017

Ohshima, K. I., Fukamachi, Y., Williams, G. D., Nihashi, S., Roquet, F., Kitade, Y., et al. (2013). Antarctic Bottom Water production by intense sea-ice formation in the Cape Darnley polynya. *Nature Geoscience*, *6*(3), 235–240. https://doi.org/10.1038/ngeo1738

Oschlies, A., Koeve, W., Rickels, W., & Rehdanz, K. (2010). Side effects and accounting aspects of hypothetical large-scale Southern Ocean iron fertilization. *Biogeosciences*, *7*(12), 4014–4035. https://doi.org/10.5194/bg-7-4017-2010

Palter, J. B., Sarmiento, J. L., Gnanadesikan, A., Simeon, J., & Slater, R. D. (2010). Fueling export production: Nutrient return pathways from the deep ocean and their dependence on the Meridional Overturning Circulation. *Biogeosciences*, *7*(11), 3549–3568. https://doi.org/10.5194/bg-7-3549-2010

Paris, C. B., Helgers, J., van Sebille, E., & Srinivasan, A. (2013). Connectivity modeling system: A probabilistic modeling tool for the multi-scale tracking of biotic and abiotic variability in the ocean. *Environmental Modelling & Software*, *42*, 47–54. https://doi.org/10.1016/j.envsoft.2012.12.006

Primeau, F. W., Holzer, M., & DeVries, T. (2013). Southern Ocean nutrient trapping and the efficiency of the biological pump. *Journal of Geophysical Research: Oceans*, *118*(5), 2547–2564. https://doi.org/10.1002/jgrc.20181

Rickels, W., Rehdanz, K., & Oschlies, A. (2012). Economic prospects of ocean iron fertilization in an international carbon market. *Resource and Energy Economics*, *34*(1), 129–150. https://doi.org/10.1016/j.reseneeco.2011.04.003

Robinson, J., Popova, E. E., Yool, A., Srokosz, M., Lampitt, R. S., & Blundell, J. R. (2014). How deep is deep enough? Ocean iron fertilization and carbon sequestration in the Southern Ocean. *Geophysical Research Letters*, *41*(7), 2489–2495. https://doi.org/10.1002/2013GL058799

Rogelj, J., Shindell, D., Jiang, K., Fifita, S., Forster, P., Ginzburg, V., et al. (2018). Mitigation pathways compatible with 1.5°C in the context of sustainable development. In V. Masson-Delmotte, P. Zhai, H. O. Poertner, D. Roberts, J. Skea, P. R. Shukla, et al. (Eds.), *Global Warming of 1.5°C. An IPCC Special Report on the impacts of global warming of 1.5°C above pre-industrial levels and related global greenhouse gas emission pathways, in the context of strengthening the global response to the threat of climate change* (pp. 93–174).

Rohr, T. (2019). Southern Ocean Iron fertilization: An argument against commercialization but for continued research amidst lingering uncertainty. *Journal of Science Policy & Governance*, *15*, 5847. https://doi.org/10.38126/JSPG150114

Ruseva, T., Hedrick, J., Marland, G., Tovar, H., Sabou, C., & Besombes, E. (2020). Rethinking standards of permanence for terrestrial and coastal carbon: Implications for governance and sustainability. *Current Opinion in Environmental Sustainability*, *45*, 69–77. https://doi.org/10.1016/j.cosust.2020.09.009

Ryan-Keogh, T. J., Thomalla, S. J., Monteiro, P. M. S., & Tagliabue, A. (2023). Multidecadal trend of increasing iron stress in Southern Ocean phytoplankton. *Science*, *379*(6634), 834–840. https://doi.org/10.1126/science.abl5237

Sarmiento, J. L., & Orr, J. C. (1991). Three-dimensional simulations of the impact of Southern Ocean nutrient depletion on atmospheric CO_2 and ocean chemistry. *Limnology & Oceanography*, *36*(8), 1928–1950. https://doi.org/10.4319/lo.1991.36.8.1928

Sarmiento, J. L., Slater, R. D., Dunne, J., Gnanadesikan, A., & Hiscock, M. R. (2010). Efficiency of small scale carbon mitigation by patch iron fertilization. *Biogeosciences*, *7*(11), 3593–3624. https://doi.org/10.5194/bg-7-3593-2010

Siegel, D. A., Devries, T., Doney, S. C., & Bell, T. (2021). Assessing the sequestration time scales of some ocean-based carbon dioxide reduction strategies. *Environmental Research Letters*, *16*(10), 104003. https://doi.org/10.1088/1748-9326/ac0be0

Smetacek, V., Klaas, C., Strass, V. H., Assmy, P., Montresor, M., Cisewski, B., et al. (2012). Deep carbon export from a Southern Ocean iron-fertilized diatom bloom. *Nature*, *487*(7407), 313–319. https://doi.org/10.1038/nature11229

Strong, A., Chisholm, S., Miller, C., & Cullen, J. (2009). Ocean fertilization: Time to move on. *Nature*, *461*(7262), 347–348. https://doi.org/10.1038/461347a

Tagliabue, A., Mtshali, T., Aumont, O., Bowie, A. R., Klunder, M. B., Roychoudhury, A. N., & Swart, S. (2012). A global compilation of dissolved iron measurements: Focus on distributions and processes in the Southern Ocean. *Biogeosciences*, *9*(6), 2333–2349. https://doi.org/10.5194/bg-9-2333-2012

Tagliabue, A., Twining, B. S., Barrier, N., Maury, O., Berger, M., & Bopp, L. (2023). Ocean iron fertilization may amplify climate change pressures on marine animal biomass for limited climate benefit. *Global Change Biology*, *29*(18), 1–11. https://doi.org/10.1111/gcb.16854

Tamsitt, V., Drake, H. F., Morrison, A. K., Talley, L. D., Dufour, C. O., Gray, A. R., et al. (2017). Spiraling pathways of global deep waters to the surface of the Southern Ocean. *Nature Communications*, *8*, 1–10. https://doi.org/10.1038/s41467-017-00197-0

The Royal Society. (2009). Geoengineering the climate: Science, governance and uncertainty report No. RS1636.

Twining, B. S., Baines, S. B., Fisher, N. S., & Landry, M. R. (2004). Cellular iron contents of plankton during the southern Ocean Iron experiment (SOFeX). *Deep Sea Research Part I: Oceanographic Research Papers*, *51*(12), 1827–1850. https://doi.org/10.1016/j.dsr.2004.08.007

Venables, H., & Moore, C. M. (2010). Phytoplankton and light limitation in the Southern Ocean: Learning from high-nutrient, high-chlorophyll areas. *Journal of Geophysical Research*, *115*(C2), C02015. https://doi.org/10.1029/2009jc005361

Wassmann, P. (1998). Retention versus export food chains: Processes controlling sinking loss from marine pelagic systems. *Hydrobiologia*, *363*(1/3), 29–57. https://doi.org/10.1023/A:1003113403096

Williams, G. D., Aoki, S., Jacobs, S. S., Rintoul, S. R., Tamura, T., & Bindoff, N. L. (2010). Antarctic bottom water from the adélie and george v land coast, East Antarctica (140–149°E). *Journal of Geophysical Research: Oceans*, *115*(C4), 1–29. https://doi.org/10.1029/2009JC005812

Xie, Y., Tamsitt, V., & Bach, L. T. (2022). Localizing the southern Ocean Biogeochemical divide. *Geophysical Research Letters*, *49*(8), 1–9. https://doi.org/10.1029/2022GL098260

Yoon, J. E., Yoo, K. C., MacDonald, A. M., Yoon, H. I., Park, K. T., Yang, E. J., et al. (2018). Reviews and syntheses: Ocean iron fertilization experiments—Past, present, and future looking to a future Korean Iron Fertilization Experiment in the Southern Ocean (KIFES) project. *Biogeosciences*, *15*(19), 5847–5889. https://doi.org/10.5194/bg-15-5847-2018

Zahariev, K., Christian, J. R., & Denman, K. L. (2008). Preindustrial, historical, and fertilization simulations using a global ocean carbon model with new parameterizations of iron limitation, calcification, and N2 fixation. *Progress in Oceanography*, *77*(1), 56–82. https://doi.org/10.1016/j.pocean.2008.01.007

References From the Supporting Information

Alderkamp, A. C., Van Dijken, G. L., Lowry, K. E., Lewis, K., Joy-Warren H, L., de Poll, W., et al. (2019). Effects of iron and light availability on phytoplankton photosynthetic properties in the Ross Sea. *Marine Ecology Progress Series*, *621*, 33–50. https://doi.org/10.3354/meps13000

Arrigo, K. R., Mills, M. M., Kropuenske, L. R., Van Dijken, G. L., Alderkamp, A. C., & Robinson, D. H. (2010). Photophysiology in two major southern ocean phytoplankton taxa: Photosynthesis and growth of *Phaeocystis antarctica* and *Fragilariopsis cylindrus* under different irradiance levels. *Integrative and Comparative Biology*, *50*(6), 950–966. https://doi.org/10.1093/icb/icq021

Asper, V. L., & Smith, W. O. (1999). Particle fluxes during austral spring and summer in the southern Ross Sea, Antarctica. *Journal of Geophysical Research*, *104*(C3), 5345–5359. https://doi.org/10.1029/1998jc900067

Baumann, M. E. M., Brandini, F. P., & Staubes, R. (1994). The influence of light and temperature on carbon-specific DMS release by cultures of Phaeocystis Antarctica and three antarctic diatoms. *Marine Chemistry*, *45*(1–2), 129–136. https://doi.org/10.1016/0304-4203(94)90097-3

Berelson, W. M. (2001). The flux of particulate organic carbon into the ocean interior: A comparison of four U.S. JGOFS regional studies. *Oceanography*, *14*(4), 59–67. https://doi.org/10.5670/oceanog.2001.07

Bertrand, E. M., Saito, M. A., Rose, J. M., Riesselman, C. R., Lohan, M. C., Noble, A. E., et al. (2007). Vitamin B12 and iron colimitation of phytoplankton growth in the Ross Sea. *Limnology & Oceanography*, *52*(3), 1079–1093. https://doi.org/10.4319/lo.2007.52.3.1079

Boyer, T., Garcia, H., Locarnini, R., Zweng, M. M., Mishonov, A. V., Reagan, J. R., et al. (2018). *World Ocean Atlas 2018*. NOAA National Centers for Environmental Information.

Buesseler, K. O. (1998). The decoupling of production and particulate export in the surface ocean. *Global Biogeochemical Cycles*, *12*(2), 297–310. https://doi.org/10.1029/97gb03366

Buesseler, K. O., Ball, L., Andrews, J., Cochran, J. K., Hirschberg, D. J., Bacon, M. P., et al. (2001). Upper ocean export of particulate organic carbon and biogenic silica in the Southern Ocean along 170°W. *Deep Research Part II: Topical Studies in Oceanography*, *48*(19–20), 4275–4297. https://doi.org/10.1016/S0967-0645(01)00089-3

Buesseler, K. O., Barber, R. T., Dickson, M. L., Hiscock, M. R., Moore, J. K., & Sambrotto, R. (2003). The effect of marginal ice-edge dynamics on production and export in the Southern Ocean along 170°W. *Deep Research Part II: Topical Studies in Oceanography*, *50*(3–4), 579–603. https://doi.org/10.1016/S0967-0645(02)00585-4

Butterworth, B. J., & Miller, S. D. (2016). Air-sea exchange of carbon dioxide in the Southern Ocean and Antarctic marginal ice zone. *Geophysical Research Letters*, *43*(13), 7223–7230. https://doi.org/10.1002/2016GL069581

Campbell, J. W., & Aarup, T. (1989). Photosynthetically available radiation at high latitudes. *Limnology & Oceanography*, *34*(8), 1490–1499. https://doi.org/10.4319/lo.1989.34.8.1490

Carter, B. R., Feely, R. A., Williams, N. L., Dickson, A. G., Fong, M. B., & Takeshita, Y. (2018). Updated methods for global locally interpolated estimation of alkalinity, pH, and nitrate. *Limnology and Oceanography: Methods*, *16*(2), 119–131. https://doi.org/10.1002/lom3.10232

Cavan, E. L., Le Moigne, F. A. C., Poulton, A. J., Tarling, G. A., Ward, P., Daniels, C. J., et al. (2015). Attenuation of particulate organic carbon flux in the Scotia Sea, Southern Ocean, is controlled by zooplankton fecal pellets. *Geophysical Research Letters*, *42*, 821–830. https://doi.org/10.1002/2014GL062744

Coale, K. H., Wang, X., Tanner, S. J., & Johnson, K. S. (2003). Phytoplankton growth and biological response to iron and zinc addition in the Ross Sea and Antarctic Circumpolar Current along 170°W. *Deep Research Part II: Topical Studies in Oceanography*, *50*(3–4), 635–653. https://doi.org/10.1016/S0967-0645(02)00588-X

Cochran, J. K., Buesseler, K. O., Bacon, M. P., Wang, H., Hirschberg, D., Ball, L., et al. (2000). Short-lived thorium isotopes (^{234}Th, ^{228}Th) as indicators of poc export and particle cycling in the ross sea, southern ocean. *Deep Research Part II: Topical Studies in Oceanography*, *47*(15–16), 3451–3490. https://doi.org/10.1016/S0967-0645(00)00075-8

Cullen, J. T., Chase, Z., Coale, K. H., Fitzwater, S. E., & Sherrell, R. M. (2003). Effect of iron limitation on the cadmium to phosphorus ratio of natural phytoplankton assemblages from the Southern Ocean. *Limnology & Oceanography*, *48*(3), 1079–1087. https://doi.org/10.4319/lo.2003.48.3.1079

Endo, H., Hattori, H., Mishima, T., Hashida, G., Sasaki, H., Nishioka, J., & Suzuki, K. (2017). Phytoplankton community responses to iron and CO_2 enrichment in different biogeochemical regions of the Southern Ocean. *Polar Biology*, *40*(11), 2143–2159. https://doi.org/10.1007/s00300-017-2130-3

Gattuso, J.-P., Epitalon, J.-M., Lavigne, H., & Orr, J. (2021). Seacarb: Seawater carbonate chemistry with R. R package version 3.0.

Gregor, L., Lebehot, A. D., Kok, S., & Scheel Monteiro, P. M. (2019). A comparative assessment of the uncertainties of global surface ocean CO_2 estimates using a machine-learning ensemble (CSIR-ML6 version 2019a)-have we hit the wall? *Geoscientific Model Development*, *12*, 5113–5136. https://doi.org/10.5194/gmd-12-5113-2019

Guidi, L., Legendre, L., Reygondeau, G., Uitz, J., Stemmann, L., & Henson, S. A. (2015). A new look at the ocean carbon remineralization for estimating deepwater sequestration. *Global Biogeochemical Cycles*, *29*(7), 1044–1059. https://doi.org/10.1002/2014GB005063

Henson, S. A., Sanders, R., Madsen, E., Morris, P. J., Le Moigne, F., & Quartly, G. D. (2011). A reduced estimate of the strength of the ocean's biological carbon pump. *Geophysical Research Letters*, *38*(4), 10–14. https://doi.org/10.1029/2011GL046735

Hopkinson, B. M., Mitchell, B. G., Reynolds, R. A., Wang, H., Selph, K. E., Measures, C. I., et al. (2007). Iron limitation across chlorophyll gradients in the southern Drake Passage: Phytoplankton responses to iron addition and photosynthetic indicators of iron stress. *Limnology & Oceanography*, *52*(6), 2540–2554. https://doi.org/10.4319/lo.2007.52.6.2540

Huang, B., Liu, C., Banzon, V., Freeman, E., Graham, G., Hankins, B., et al. (2021). Improvements of the daily optimum interpolation sea surface temperature (DOISST) version 2.1. *Journal of Climate*, *34*(8), 2923–2939. https://doi.org/10.1175/JCLI-D-20-0166.1

Jones, D. C., Ito, T., Takano, Y., & Hsu, W. C. (2014). Spatial and seasonal variability of the air-sea equilibration timescale of carbon dioxide. *Global Biogeochemical Cycles*, *28*(11), 1163–1178. https://doi.org/10.1002/2014GB004813

Katlein, C., Arndt, S., Belter, H. J., Castellani, G., & Nicolaus, M. (2019). Seasonal evolution of light transmission distributions through Arctic Sea Ice. *Journal of Geophysical Research: Oceans*, *124*(8), 5418–5435. https://doi.org/10.1029/2018JC014833

Kustka, A. B., Jones, B. M., Hatta, M., Field, M. P., & Milligan, A. J. (2015). The influence of iron and siderophores on eukaryotic phytoplankton growth rates and community composition in the Ross Sea. *Marine Chemistry*, *173*, 195–207. https://doi.org/10.1016/j.marchem.2014.12.002

Langone, L., Frignani, M., Cochran, J. K., & Ravaioli, M. (1997). Scavenging processes and export fluxes close to a retreating seasonal ice margin (Ross Sea, Antarctica). In D. Evans, J. Wisniewski, & J. Wisniewski (Eds.), *The interactions between sediments and water* (pp. 705–715). Springer.

Laws, E. A., & Maiti, K. (2019). The relationship between primary production and export production in the ocean: Effects of time lags and temporal variability. *Deep-Sea Research Part I Oceanographic Research Papers*, *148*, 100–107. https://doi.org/10.1016/j.dsr.2019.05.006

Le Moigne, F. A. C., Henson, S. A., Cavan, E., Georges, C., Pabortsava, K., Achterberg, E. P., et al. (2016). What causes the inverse relationship between primary production and export efficiency in the Southern Ocean? *Geophysical Research Letters*, *43*(9), 4457–4466. https://doi.org/10.1002/2016GL068480

Maslanik, J., & Stroeve, J. (1999). Near-real-time DMSP SSM/I-SSMIS daily polar gridded sea ice concentrations.

Millero, F. J., Graham, T. B., Huang, F., Bustos-Serrano, H., & Pierrot, D. (2006). Dissociation constants of carbonic acid in seawater as a function of salinity and temperature. *Marine Chemistry*, *100*(1–2), 80–94. https://doi.org/10.1016/j.marchem.2005.12.001

Mobley, C. D., & Boss, E. S. (2012). Improved irradiances for use in ocean heating, primary production, and photo-oxidation calculations. *Applied Optics*, *51*(27), 6549–6560. https://doi.org/10.1364/AO.51.006549

Öztürk, M., Croot, P. L., Bertilsson, S., Abrahamsson, K., Karlson, B., David, R., et al. (2004). Iron enrichment and photoreduction of iron under UV and PAR in the presence of hydroxycarboxylic acid: Implications for phytoplankton growth in the Southern Ocean. *Deep Research Part II: Topical Studies in Oceanography*, *51*(22–24), 2841–2856. https://doi.org/10.1016/j.dsr2.2000.10.001

Prytherch, J., Brooks, I., Crill, P., Thornton, B. F., Salisbury, D. J., Tjernström, M., et al. (2017). Direct determination of the air-sea CO_2 gas transfer velocity in Arctic sea ice regions. *Geophysical Research Letters*, *44*(8), 3770–3778. https://doi.org/10.1002/2017GL073593

Rodriguez y Baena, A. M., Boudjenoun, R., Fowler, S. W., Miquel, J. C., Masqué, P., Sanchez-Cabeza, J. A., & Warnau, M. (2008). ^{234}Th-based carbon export during an ice-edge bloom: Sea-ice algae as a likely bias in data interpretation. *Earth and Planetary Science Letters*, *269*(3–4), 596–604. https://doi.org/10.1016/j.epsl.2008.03.020

Rose, J. M., Feng, Y., Ditullio, G. R., Dunbar, R. B., Hare, C. E., Lee, P. A., et al. (2009). Synergistic effects of iron and temperature on Antarctic phytoplankton and microzooplankton assemblages. *Biogeosciences*, *6*(12), 3131–3147. https://doi.org/10.5194/bg-6-3131-2009

Rutgers van der Loeff, M., Cai, P. H., Stimac, I., Bracher, A., Middag, R., Klunder, M. B., & van Heuven, S. M. A. C. (2011). ^{234}Th in surface waters: Distribution of particle export flux across the Antarctic Circumpolar Current and in the Weddell Sea during the GEOTRACES

expedition ZERO and DRAKE. *Deep Research Part II: Topical Studies in Oceanography*, *58*(25–26), 2749–2766. https://doi.org/10.1016/j.dsr2.2011.02.004

Sedwick, P. N., Di Tullio, G. R., & Mackey, D. J. (2000). Iron and manganese in the Ross Sea, seasonal iron limitation in antarctic. *Journal of Geophysical Research: Oceans*, *105*(C5), 11321–11336. https://doi.org/10.1029/2000JC000256

Sedwick, P. N., Garcia, N. S., Riseman, S. F., Marsay, C. M., & DiTullio, G. R. (2007). Evidence for high iron requirements of colonial Phaeocystis Antarctica at low irradiance. *Biogeochemistry*, *83*(1–3), 83–97. https://doi.org/10.1007/s10533-007-9081-7

Shimmield, G. B., Ritchie, G. D., & Fileman, T. W. (1995). The impact of marginal ice zone processes on the distribution of ^{21}OPb, ^{21}OPo and ^{234}Th and implications for new production in the Bellingshausen Sea, Antarctica. *Deep. Res. Part II*, *42*(4–5), 1313–1335. https://doi.org/10.1016/0967-0645(95)00071-W

Silsbe, G. M., Behrenfeld, M. J., Halsey, K. H., Milligan, A. J., & Westberry, T. K. (2016). The CAFE model: A net production model for global ocean phytoplankton. *Global Biogeochemical Cycles*, *30*(12), 1756–1777. https://doi.org/10.1002/2016GB005521

Strzepek, R. F., Hunter, K. A., Frew, R. D., Harrison, P. J., & Boyd, P. W. (2012). Iron-light interactions differ in Southern Ocean phytoplankton. *Limnology & Oceanography*, *57*(4), 1182–1200. https://doi.org/10.4319/lo.2012.57.4.1182

Takeda, S. (1998). Influence of iron availability on nutrient consumption ratio. *Nature*, *393*(6687), 774–777. https://doi.org/10.1038/31674

Timmermans, K. R., Van Leeuwe, M. A., De Jong, J. T. M., McKay, R., Nolting, R., Witte, H., et al. (1998). Iron stress in the Pacific region of the Southern Ocean: Evidence from enrichment bioassays. *Marine Ecology Progress Series*, *166*, 27–41. https://doi.org/10.3354/meps166027

Timmermans, K. R., Veldhuis, M. J. W., & Brussaard, C. P. D. (2007). Cell death in three marine diatom species in response to different irradiance levels, silicate, or iron concentrations. *Aquatic Microbial Ecology*, *46*, 253–261. https://doi.org/10.3354/ame046253

Van Leeuwe, M. A., Scharek, R., De Baar, H. J. W., De Jong, J. T. M., & Goeyens, L. (1997). Iron enrichment experiments in the Southern Ocean: Physiological responses of plankton communities. *Deep Research Part II: Topical Studies in Oceanography*, *44*(1–2), 189–207. https://doi.org/10.1016/S0967-0645(96)00069-0

Viljoen, J. J., Philibert, R., Van Horsten, N., Mtshali, T., Roychoudhury, A. N., Thomalla, S., & Fietz, S. (2018). Phytoplankton response in growth, photophysiology and community structure to iron and light in the Polar Frontal Zone and Antarctic waters. *Deep Research Part II: Topical Studies in Oceanography*, *141*, 118–129. https://doi.org/10.1016/j.dsr.2018.09.006

Wanninkhof, R. (2014). Relationship between wind speed and gas exchange over the ocean revisited. *Limnology and Oceanography: Methods*, *12*(6), 351–362. https://doi.org/10.4319/lom.2014.12.351

Wentz, F. J., Scott, J., Hoffman, R., Leidner, M., Atlas, R., & Ardizzone, J. (2015). *Remote sensing systems Cross-Calibrated Multi-Platform (CCMP) 6-hourly ocean vector wind analysis product on 0.25 deg grid, Version 2.0*. Remote Sensing System.

Wu, M., McCain, J. S. P., Rowland, E., Middag, R., Sandgren, M., Allen, A. E., & Bertrand, E. M. (2019). Manganese and iron deficiency in Southern Ocean Phaeocystis Antarctica populations revealed through taxon-specific protein indicators. *Nature Communications*, *10*, 1–10. https://doi.org/10.1038/s41467-019-11426-z